Structure-function dissection of the Pseudorabies virus glycoprotein B fusion loops

Melina Vallbracht, Delphine Brun, Matteo Tassinari, Marie-Christine Vaney, Gerard Pehau-Arnaudet, Pablo Guardado-Calvo, Ahmed Haouz, Barbara G. Klupp, Thomas C. Mettenleiter, Félix A. Rey, et al.

Structure-function dissection of the Pseudorabies virus glycoprotein B fusion loops

Melina Vallbracht[a], Delphine Brun[b,c], Matteo Tassinari[b,c,*], Marie-Christine Vaney[b,c], Gérard Pehau-Arnaudet[d,e], Pablo Guardado-Calvo[b,c], Ahmed Haouz[e,f], Barbara G. Klupp[a], Thomas C. Mettenleiter[a], Felix A. Rey[b,c], Marija Backovic [#,b,c]

Institute of Molecular Virology and Cell Biology, Friedrich-Loeffler-Institut, Greifswald-Insel Riems, Germany[a]; Institut Pasteur, Unité de Virologie Structurale, Département de Virologie, Paris, France[b]; CNRS UMR3569, Paris, France[c]; Institut Pasteur, Ultrapole, Département de Biologie Cellulaire et Infection, Paris, France[d]; CNRS UMR3528, Paris, France[e]; Institut Pasteur, Plate-forme de Cristallographie[f].

Running title: PrV gB ectodomain – structure-based mutagenesis

#Address correspondence to Marija Backovic, marija@pasteur.fr.

[*]Present address : Institut Pasteur, Unité de Microbiologie Structurale, Département de biologie structurale et chimie, Paris, France.

Word count: abstract (248), text (8,554).

ABSTRACT:

Conserved across the *Herpesviridae* family, glycoprotein B (gB) is responsible for driving fusion of the viral envelope with the host cell membrane for entry upon receptor binding and activation by the viral gH/gL complex. Although crystal structures of the gB ectodomain of several herpesviruses have been reported, the membrane fusion mechanism has remained elusive. Here, we report the X-ray structure of the Pseudorabies virus (PrV) gB ectodomain, revealing a typical class III post-fusion trimer that binds membranes via its fusion loops (FLs) in a cholesterol-dependent manner. Mutagenesis of FL residues allowed us to dissect those interacting with distinct sub-regions of the lipid bilayer and their role for membrane interactions. We tested 15 gB variants for their ability to bind to liposomes, and further investigated a subset of them in functional assays. We found that PrV gB FL residues *Trp187, Tyr192, Phe275* and *Tyr276,* which were essential for liposome binding and for fusion in a cellular and viral context, form a continuous hydrophobic patch at the gB trimer surface. Together with reported results from other alpha-herpesvirus gBs, our data suggest a model in which *Phe275* from the tip of FL2 protrudes deeper into the hydrocarbon core of the lipid bilayer, while the side chains of *Trp187, Tyr192* and *Tyr276* form a rim that inserts into the more superficial, interfacial region of the membrane to catalyze the fusion process. Comparative analysis with gB from beta- and gamma-herpesviruses suggest that this membrane-interaction mode is valid for gB from all herpesviruses.

40 **IMPORTANCE:**

41 Herpesviruses are common human and animal pathogens, which infect cells by entering via
42 fusion of viral and cellular membranes and which cause life-long and incurable infections.
43 Central to the membrane fusion event for entry is glycoprotein B (gB), which is the most
44 conserved envelope protein across the herpesvirus family. Like other viral fusion proteins, gB
45 anchors itself into the target membrane via two polypeptide segments called fusion loops (FL).
46 The molecular details of how gB FLs insert into the lipid bilayer have not been described. We
47 provide here structural and functional data regarding key FL residues of gB from *Pseudorabies*
48 *virus*, a porcine herpesvirus of veterinary concern, which allows us to propose, for the first time,
49 a molecular model to understand how the initial interactions by gB from all herpesviruses with
50 target membranes are established.

INTRODUCTION

The family *Herpesviridae* contains a large number of enveloped, double-stranded DNA viruses, which are classified into alpha-, beta-, and gamma-herpesvirus subfamilies based on their evolutionary relationship and biological properties (1). Pseudorabies virus (Suid alphaherpesvirus 1), the etiological agent of Aujeszky's disease in swine (2), belongs to the *Alphaherpesvirinae*, which also includes human pathogens such as herpes simplex virus 1 and 2 (HSV-1, HSV-2) and varicella zoster virus (VZV). PrV has been a useful model for studying the biology of alphaherpesviruses in general (3).

Herpesviruses enter cells by fusion of their envelope with the host cell plasma membrane or with the membrane of an endocytic vesicle, depending on the virus and the cell type (4, 5). While many enveloped viruses require only one or two proteins to mediate receptor binding and entry, herpesviruses rely on the concerted action of at least four glycoproteins. Distinct viral proteins first engage specific cellular receptors in an interaction that provides a trigger for membrane fusion (e.g. glycoprotein D (gD) in HSV-1/-2 and PrV, gO in the beta-herpesvirus human cytomegalovirus (HCMV), gp42 in the gamma-herpesvirus Epstein-Barr virus (EBV)) (6-9). The merger of the viral and cellular membranes is then catalyzed by a fusion machinery, which is conserved across the herpesvirus family and consists of gB and a heterodimeric complex of membrane-bound gH in association with the anchorless gL (gH/gL) (reviewed in (10, 11)).

The molecular basis of the entry mechanism has been best described for alphaherpesviruses. In HSV-1, the cascade begins with gD binding to cellular receptors such as herpesvirus entry mediator (HVEM), nectin-1 or 3-O-sulfonated heparin sulfate (reviewed in

(12)). This interaction leads to a conformational change in gD (13, 14) that is believed to enable its interaction with the gH/gL complex, which in turn triggers gB to carry out membrane fusion (15, 16). It should be noted that unlike HSV-1, PrV does not require gD for direct viral cell-cell spread and gB-induced cell:cell fusion (17-19). Moreover, PrV virions can acquire the ability to infect cells in the absence of gD, gL or the N-terminal domain of gH, by compensatory mutations in other envelope glycoproteins (20, 21).

gB was proposed to be the *bona fide* fusion protein of herpesviruses due to its structural homology with the fusogenic G protein of the otherwise unrelated vesicular stomatitis virus (VSV) (22). Together with VSV G and the baculovirus fusion protein gp64 (23), gB was classified as a class III fusion protein. Viral fusion proteins are in general presented in a metastable pre-fusion state on the viral membrane. Upon an activation signal they undergo conformational rearrangements unmasking the initially buried hydrophobic regions (fusion peptide (FP) or fusion loop(s) (FL)) for interactions with the target membrane, resulting in simultaneous anchorage of the fusion protein in the viral and cellular membrane at opposite ends of the protein. This extended intermediate is unstable and rapidly folds back into a “hairpin”, an energetically more favorable post-fusion conformation (24, 25).

gB is the most conserved envelope glycoprotein of herpesviruses, although only ≈5% of its residues are identical across the entire herpesvirus family. The level of conservation is higher within each subfamily, and PrV and HSV-1 gB share 50% amino acid sequence identity. The X-ray structures determined for the post-fusion gB ectodomains from HSV-1 (26), EBV (27) and HCMV (28, 29) demonstrate conservation of the three-dimensional structural organization. Although the crystal structure of gB in a pre-fusion state has not been determined yet, a low-

95 resolution structure of full-length HSV-1 gB in an intermediate state different from the post-
96 fusion conformation was obtained by cryo-electron tomography (30). VSV G protein has been
97 crystallized in both pre- and post-fusion conformations. The former revealed a trimeric
98 molecule with the FLs pointing towards the viral membrane, and with a different spatial
99 organization of domains compared to the post-fusion, low pH form (31). Hypothetical models of
100 the pre-fusion gB using the VSV G conformation as a template have been proposed (27, 32), but
101 supporting structural data are still lacking. The high structural conservation observed for gB also
102 applies to the gH/gL complex as illustrated by the X-ray structures of the gH/gL ectodomains
103 from HSV-2, EBV, VZV, and a core domain of PrV gH (33-36), which reveal a common fold
104 despite low sequence conservation (37). gH/gL has no structural resemblance to any known
105 fusion protein but was shown to play a role in regulation of the fusion activity of gB (37, 38).
106 Membrane-interacting regions of fusion proteins are typically well conserved within the
107 virus family, and are rich in hydrophobic and aromatic residues that insert into the outer leaflet
108 of a cell membrane (39). In class I fusion proteins, they are called FPs, which can be N-terminal
109 peptides or an internal loop near the N-terminus, as in the Ebola envelope glycoprotein GP2 for
110 example (40) (to avoid confusion, we reserve the term FL for the loops of class II and III fusion
111 proteins, and we refer to all class I membrane interacting regions as fusion peptides, even when
112 they correspond to an internal loop). FPs were shown to adopt a different structure upon
113 insertion into target membranes (reviewed in (41)). The FLs of class II and class III fusion
114 proteins, in contrast, are conformationally constrained by being a part of a larger structured β-
115 barrel domain, and appear to largely maintain their structure upon membrane insertion. In
116 class II fusion proteins, the membrane interacting surface can be composed of residues from

one (flaviviruses and alphaviruses (42, 43)), two (rubella virus, pheloboviruses (44, 45)) or three FLs (hantaviruses (46)), while the known class III fusion proteins use two FLs to interact with membranes. FLs of herpesviruses are unusual because their amino acid sequence is poorly conserved even within subfamilies. Therefore, their identification was impossible until structural data became available. Residues exposed at the tips of the recombinant crystallized HSV-1 gB ectodomain (26) were proposed to form the FLs based on structural homology with the well-defined FLs of the VSV G protein (47, 48). A similar organization of the FLs was observed in the reported gB structures, with the difference that the aromatic and apolar residues are predominantly presented at the sides of the HSV-1 FLs, while they protrude from the tips of the EBV and HCMV FLs. These exposed hydrophobic residues in EBV and HCMV gB caused the recombinant ectodomains to aggregate, forming rosette-like structures (49, 50). Mutagenesis of the hydrophobic residues within the FL, while abolishing their fusion function, was essential for solubility of these proteins for structure determination (50, 51). In contrast, HSV-1 gB (52), and PrV gB (this study) exhibit less hydrophobic tips, form soluble trimers, and can be studied and crystallized as functional, wild type proteins.

Extensive mutagenesis studies have been performed on HSV-1 gB, demonstrating that the hydrophobic residues *Trp174*, *Phe175*, *Tyr179* in FL1, and *Ala261* in FL2 as well as polar and charged residues, such as *His263* and *Arg264* presented at the sides of FL2, play an important role in fusion (52-55). The hydrophobic residues were proposed to form a patch that inserts into the membrane, while the *His* and *Arg* side chains were speculated to interact with phospholipid head groups without penetrating deeper into the membrane. In support of this model, the low-resolution structure of HSV-1 gB ectodomains bound to liposomes and obtained

139 by cryo-electron tomography, showed that the interactions of the HSV-1 gB ectodomains are
140 limited to the outer membrane leaflet. This model predicted that the FLs would insert into the
141 bilayer at an oblique angle indicating that the residues from β-strands leading to the FLs may be
142 involved in the interactions with lipids (56). HSV-1 gB FL residues *Trp174*, *Tyr179*, *His263* and
143 *Arg264* were furthermore shown to be the contact sites for interactions of the ectodomain with
144 liposomes (55).

145 Cholesterol (CH) is a lipid that is ubiquitously present in mammalian cell membranes,
146 where it plays an important role in entry of many viruses (57), including PrV and HSV-1
147 (reviewed in (58-60)). The HSV-1 gB ectodomain was shown to bind to liposomes only in the
148 presence of cholesterol (55), and full-length HSV-1 gB expressed in cells was found to associate
149 with lipid rafts (61).

150 While the current HSV-1 model has provided an important step forward in
151 understanding how gB binds to membranes, it has been unclear whether a similar model of
152 insertion would hold true for other gB proteins due to the poor conservation of the FLs,
153 highlighting the need to study each gB individually and to perform comparative analyses. With
154 this in mind, we sought to enlarge the structural and functional repertoire available for
155 alphaherpesviruses by carrying out studies on PrV gB. We report here the X-ray crystal
156 structure of the PrV gB ectodomain at 2.7Å resolution, and demonstrate that the recombinant
157 ectodomains bind to liposomes in a cholesterol-dependent fashion. The association with
158 liposomes occurs via the trimer tip that contains the FLs, resembling the shallow insertion
159 observed for HSV-1 gB. We designed the PrV gB mutagenesis to complement what had been
160 already reported for HSV-1 gB, and to target all aromatic and hydrophobic residues within the

FLs, some of which are unique to PrV and some that are conserved in HSV-1 gB as well. The resulting pattern of active and inactive FL mutants matches in part what had been observed previously for HSV-1 gB, but with some interesting differences that shine a new light on the way the FLs insert into membranes. Based on our results, we propose a model in which the tip of FL2 penetrates deeper into the lipid bilayer reaching into the hydrophobic core, while residues on the sides of the FL1 and FL2 tips position their side chains within the same plane, inserting into the amphipathic, interfacial region of the membrane. Comparative analysis with the FLs of HCMV and EBV gB further suggests that in spite of considerable sequence divergence, this model could be used to describe in general the way gB interacts with membranes for all herpes viruses.

RESULTS

PrV gB expression, crystallization and structure determination.

The ectodomain expression construct of PrV gB (Suid alphaherpesvirus 1, Kaplan strain, GenBank number AEM64049.1) encodes for residues 59-756 (Fig. 1A). The construct was designed to exclude the gB signal sequence (residues 1-58), which was replaced by the *Drosophila* Bip signal peptide, present in the expression vector and known to drive efficient expression of heterologous proteins (62). The expression construct ends with the double strep affinity tag added just before the hydrophobic membrane proximal region (MPR) (residues 757 – 800), which is followed by the transmembrane region (residues 801 - 821) and the cytoplasmic domain (residues 822 - 916) in the intact protein.

182 The PrV gB ectodomain was expressed using stably transfected *Drosophila* Schneider 2
183 (S2) cell lines as described (63). After affinity and size exclusion chromatography (SEC), we
184 obtained 8-12 milligrams of pure protein from 1 liter of cell culture. The protein eluted as a
185 single peak from a SEC column, and exhibited no signs of aggregation. SDS-PAGE analysis of the
186 purified ectodomain showed a single band migrating just below the 100kDa marker under non-
187 reducing conditions (Fig. 1B, lane 1). PrV gB contains a furin cleavage site ^{501}RRARR^{505}, and the
188 recombinant protein is cleaved by furin in S2 cells as demonstrated by the presence of two
189 protein bands of lower molecular masses under reducing conditions (~60kDa and ~40kDa
190 fragments labeled, respectively, as gB^{b} and gB^{c}) (Fig. 1B, lane 3).
191 Compared to its 100kDa apparent molecular mass, the polypeptide chain of the gB
192 ectodomain has a calculated mass of 82kDa, corresponding to the 49kDa N-terminal and 33kDa
193 C-terminal furin cleavage products, which indicates the presence of post-translational
194 modifications in the mature protein. There are six predicted N-glycosylation sites (four in the N-
195 terminal and two in the C-terminal fragment), and a shift to a lower molecular mass is indeed
196 observed for both fragments upon treatment with a deglycosidase (Fig. 1B, lanes 2 and 4).
197 *Drosophila* S2 cells add 1-2kDa simple mannose core structures to form N-linked sugars (64),
198 accounting for the presence of several N-linked sugars in the expressed protein.
199 The purified gB ectodomains crystallized easily under numerous conditions, but the
200 crystals were fragile and of poor diffraction quality. Upon enzymatic deglycosylation with Endo
201 D, we obtained diffraction-quality crystals in 0.1M Tris pH 8.5, 7% PEG 4,000, 0.6M LiCl.
202 Diffraction data were collected and processed as described in the Material and Methods
203 section. The crystals belong to the H3 space group (a=99.9Å, b=99.9Å, c=272.9Å; α=β=90°,

γ=120°), with one gB protomer per asymmetric unit. Crystallographic statistics of data processing and structure refinement are given in Table 1.

PrV gB forms a typical class III post-fusion trimer.

The PrV gB ectodomain folds into an ~16 nm x ~8 nm trimeric spike, resembling the structures reported for the postulated post-fusion conformation of the HSV-1 (26), EBV (27) and HCMV gB ectodomains (28, 29). Briefly, the N-terminus of the protein (amino acid 113) is located at the top end of the trimer, with the polypeptide chain running down along the entire length of the spike, folding into domain I, which carries the FLs exposed at the base of the molecule (Fig. 1C). Domain II is positioned laterally, adopting a fold reminiscent of the pleckstrin homology domains. The furin cleavage site is located in the flexible linker that connects domains II and III, and could not be resolved in our structure. Domain III contains the prominent, centrally located helix that extends to the top of the molecule, followed by domain IV, also known as the 'top' or 'crown' domain. The residues 697-750 form a stretched chain that packs tightly into the crevice formed by the other two protomers. This so-called 'domain V' has the appearance of a zipper that seals the trimer (Fig. 1D), resulting in the C-terminus of the ectodomain (amino acid 750) being brought into close vicinity of the FLs.

Although the expression construct encodes for gB residues 59-756, the first residue resolved in the crystal structure was *Arg113*, consistent with the highly flexible N-terminal end of the protein, which is rich in glycine and proline residues. The same applies to HSV-1, EBV and HCMV gB, in which the N-terminal region of the crystallized construct was not resolved either. The other PrV gB regions that were not built into the structure are the above mentioned

unstructured segment that contains the furin cleavage site and connects domains II and III (residues 478-521), and the C-terminal six residues of the ectodomain (residues 750-756), which are followed by the double strep tag in the expression construct. The PrV gB structure, however, does reveal 3 residues at the very N-terminus (residues 113-116), which had not been observed in the other gB structures. This segment forms a short β-strand (β1) in domain IV that packs against β29 in an anti-parallel fashion (Fig. 1C, 1D).

Of six potential N-glycosylation sites, we observed density for the sugar moieties attached to *Asn264* (domain I), *Asn444* (domain II) and *Asn636* (domain IV). The electron density was of sufficient quality to allow placing one an N-acetyl glucosamine (NAG) residue only to *Asn264* (Fig. 1C and D).

As anticipated, PrV gB shows higher structural conservation with the HSV-1 homolog than with the more distant gB of EBV or HCMV. The root-mean-square deviation (rmsd) for the superposition of the PrV and HSV-1 structures is 1.04 Å for Cα atoms (Table 3). The main difference between the PrV and HSV-1 ectodomains, regarding the gross organization of the spike, resides in the position of domain IV, which appears slightly rotated when the structures are superposed on domains I and II. Domain IV disposition is even more evident when compared to HCMV and EBV gB (Fig. 2).

PrV gB ectodomain requires cholesterol in the membrane for binding.

The recombinant PrV gB ectodomain used for crystallization was tested for binding to liposomes of different composition in co-floatation experiments in density gradients, as described in detail in Materials and Methods. Briefly, the protein-liposome mixture, adjusted to

248 36% iodixanole (Optiprep), was loaded below the 20% iodixanole layer that was then overlaid
249 with buffer and subjected to ultracentrifugation. Liposomes float and are found at the top of
250 the gradient, while the protein alone sediments and remains at the bottom of the tube. Protein
251 bound to liposomes co-floats with liposomes, and in this case partitions to the top of the
252 gradient. All gradient fractions were analyzed for presence of the protein in the control
253 experiments, demonstrating that gB was found either at the top or bottom of the gradient,
254 which is why only these two fractions were analyzed further.

255 Liposomes containing 60% 1,2-dioleoyl-*sn*-glycero-3-phosphocholine (DOPC) and 40%
256 cholesterol (CH) were prepared. This is the same composition used for testing HSV-1 gB
257 ectodomain interactions with membranes (55, 65). The top and bottom faction were analyzed
258 by Western blot (WB) with a reagent that specifically binds to the strep affinity tag. WT PrV gB
259 ectodomain was found in the top fraction only when liposomes were present, and sedimented
260 to the bottom of the tube in the absence of liposomes (Fig. 3A). Complexes made of WT PrV gB
261 ectodomain and liposomes containing DOPC and increasing molar amounts of CH (100% DOPC,
262 80% DOPC + 20% CH, or 60% DOPC + 40% CH) were prepared and tested next. gB ectodomains
263 bound only to the latter type of liposomes (Fig. 3B), suggesting that there is a threshold in CH
264 concentration required for the association. To determine if the lack of binding at lower CH
265 concentrations was due to the requirement for another lipid rather than insufficient CH
266 concentration, a series of liposomes made of mixtures of DOPC, 1,2-dioleoyl-sn-glycero-3-
267 phosphoethanolamine (DOPE), and sphingomyelin (SM) was prepared in the presence of 40%
268 CH, or without CH. DOPE alone or mixed with CH does not form liposomes, but assembles into
269 lipid nanotubes due to its inverted hexagonal shape (66), which is why these lipid mixtures

were omitted. The results of the floatation experiments showed that WT gB was present in the top fraction i.e. bound to the liposomes only in the presence of CH (Fig. 3C), reinforcing the conclusion that CH is essential for PrV gB ectodomain interactions with liposomes.

A sample of gB mixed with liposomes was visualized by negative stain electron microscopy (EM) (Fig. 4A), revealing liposomes decorated by protein arrays, forming honeycomb-like structures in which the individual trimers appear to be in contact with each other. Cryo-EM images of the same sample (Fig. 4B) showed individual gB trimers packing tightly and inserting into the liposomes via the spike end that contains the FLs (domain I), as was observed for the HSV-1 protein (56).

Selection of PrV gB FL residues and design of mutagenesis studies.

The side chains of *Trp* and *Phe*, as well as smaller hydrophobic residues such as *Leu* or *Ile* have favorable energies for penetration into the hydrophobic membrane core, made exclusively of lipid tails (67), while amphipathic *Tyr* and *His* side chains preferentially partition in the interfacial membrane region, localized between the hydrocarbon core and the aqueous phase (67, 68). *Trp* is also often found in this region (69). The interfacial membrane region is amphipathic itself due to the presence of carbons from the beginnings of the apolar lipid tails and of polar phosphate and glycerol groups (70). A *Phe* side chain can penetrate into the membrane core, and could thus be emulated by *Trp* but not by *Tyr* due to the presence of a polar hydroxyl group at the distal tip of the side chain. The interfacial region on the other hand would be expected to accommodate aromatic residues as *Tyr, Trp, Phe* or *His* (the latter in its unprotonated form).

292 To shed light on how the side chains of individual FL residues interact with membranes,
293 several changes were introduced: each of the aromatic or hydrophobic residues found in PrV gB
294 FLs (*Trp187*, *Tyr192*, *Tyr267*, *Ile270*, *Phe275*, *Tyr276,* and *His277*) (Fig. 5) was individually
295 mutated to *Ala*, a change that resulted in the replacement of the bulky hydrophobic side chain
296 for a methyl group, or to a different aromatic residue with similar chemical structure: *Trp* was
297 changed to *Phe* or *His*; *Phe* to *Trp* or *Tyr; His* to *Trp*, and *Tyr* to *Phe* (Table 2). This was done to
298 probe if the residue was more likely to insert deeper into the hydrocarbon core or remain in the
299 polar region of the membrane. Three of the mutagenized residues are unique to PrV gB *(Ile270,*
300 *Tyr276,* and *His277), Tyr267* is conserved but has not been mutated, and the changes
301 introduced at the conserved positions have not been analyzed earlier.
302
303 **Side chains of PrV gB FL residues *Trp187*, *Tyr192*, *Phe275* and *Tyr276* mediate binding to**
304 **liposomes and form a hydrophobic patch.**
305 To facilitate generation of mutant proteins, recombinant PrV gB ectodomains were
306 expressed after transient transfection of Expi293F mammalian cells, and the same type of
307 liposomes (60% DOPC and 40% CH) was used in the liposome floatation assay as reported for
308 the HSV-1 gB ectodomain variants (55). The variants did not differ from the WT protein in terms
309 of expression yields, behavior during affinity and size exclusion chromatography, and cleavage
310 by cellular furin (Fig. 6).
311 Substitution of the selected residues to alanine had three consequences (Table 2, Fig.
312 7A). W187A, Y192A, F275A and Y276A variants completely lost the ability to bind to liposomes
313 and were present exclusively in the bottom fraction. I270A and H277A floated as the WT

314 protein, indicating that the mutation exerted no effect on liposome binding. Y267A showed an
315 intermediate behavior, with very low binding to liposomes, at the limit of the WB detection.
316 Mutation to other aromatic residues also had different outcomes. *Trp187* was essential
317 for association of the ectodomain with liposomes, and changes to *Phe* or *His* yielded a protein
318 that did not co-float with liposomes. Y192F was only weakly detected in the liposome fraction,
319 similar to what was observed for Y267A, while Y267F and F275W bound to liposomes
320 comparable to WT gB. Interestingly, in contrast to F275W, F275Y did not associate with
321 liposomes, indicating that the presence of the hydroxyl group in F275Y may impair the ability of
322 the protein to interact with lipids. Y276F showed very weak binding, resembling Y192F and
323 Y267A. The amino acid at position 277 does not seem to be important for liposome binding,
324 since the substitutions H277A and H277W had no effect (Fig. 7A).
325 The four residues *Trp187, Tyr192, Phe275* and *Tyr276* that did not tolerate substitutions
326 to alanine, and must have a bulky aromatic side chain in order to bind to liposomes, form a
327 continuous hydrophobic and electrostatically neutral patch at the surface of the trimeric post-
328 fusion spike as shown in Fig. 7B. The phenyl group of *Phe275* appears the most protruding,
329 while *Trp187*, *Tyr192* and *Tyr276* form a rim above (Fig. 5B).
330
331 **PrV gB FL variant binding to liposomes correlates with fusion activity.**
332 The fusogenic potential of a subset of PrV gB FL mutants, including all the *Ala* variants,
333 was assessed in eukaryotic cells using the corresponding full-length gB constructs, generated by
334 site directed mutagenesis of pcDNA-gB Ka. Correct mutagenesis was verified by sequencing,
335 and protein expression and processing were analyzed, respectively, by indirect

336 immunofluorescence of permeabilized gB expressing cells (Fig. 8A) and WB of whole cell lysates
337 (Fig. 8B). The PrV gB FL variants revealed WT-like behavior both in subcellular localization and
338 processing by furin, with the exception of W187A and Y192A gB. These two variants
339 accumulated in larger structures in the cytoplasm and showed impaired furin-cleavage as
340 indicated by lower levels of the furin-cleaved subunit (gB^b) and more abundant uncleaved gB
341 (gB^a) (Fig. 8B).

342 To test the fusogenic potential of the mutated gB proteins, RK13 cells were co-
343 transfected with plasmids encoding WT gB (Ka) or the mutated gB, and gH/gL as described (71,
344 72). In addition, an enhanced green fluorescent protein (EGFP) expression plasmid was co-
345 transfected to facilitate evaluation of the assays by fluorescence microscopy (73). Transfection
346 with plasmids encoding the WT proteins served as positive control and the results were set as
347 100%, while the empty expression vector pcDNA3 was used as negative control.

348 Fusion assays revealed a good correlation between the ability of the protein to bind to
349 liposomes *in vitro*, and its activity in fusion (Table 2, Fig. 9A). Most of the variants that did not
350 show association with liposomes were unable to induce cell-cell fusion, and all variants with
351 liposome-binding properties supported efficient cell-cell fusion. Surprisingly, the three variants
352 that showed only weak binding to liposomes, Y192F, Y267A and Y276F, mediated fusion to a
353 similar extent as the WT gB.

354 To test whether this discrepancy was due to the liposome composition used in the *in*
355 *vitro* experiments (60% DOPC, 40% CH, referred to as '2L' for two lipids present), , the co-
356 floatation experiments were repeated with liposomes whose composition resembles better the
357 composition of the plasma membrane (20% DOPC, 20% DOPE, 20% SM and 40% cholesterol,

358 referred to as '4L' for four lipids present) (74-76). The three variants, Y192F, Y267A and Y276F,
359 indeed floated with '4L' liposomes like the WT protein (Fig. 9B), demonstrating that the
360 previously observed weak association was due to the inadequate liposome composition, and
361 not the mutated protein. The association of the other FL variants did not change as a function
362 of liposome composition (Fig. 9C). This data for the first time demonstrates significant
363 differences in capabilities of gB mutants to bind to liposomes as a function of lipid composition,
364 underlining the importance of testing different liposome compositions and cross-checking
365 biochemical with functional data.

366 Since W187A and Y192A variants were inactive, and showed impaired furin cleavage, we
367 wanted to establish whether furin-processing was important for the function of PrV gB in the
368 particular functional assays used in this study. A gB variant with a 5-residue deletion (RRARR) in
369 the furin site (gB-Δfurin) was created. WB analysis of gB-Δfurin expressed in RK13 cells
370 confirmed that the protein was not cleaved as indicated by a prominent band for uncleaved gB
371 (gB^a), and absence of bands corresponding to the furin-cleaved subunits (Fig. 10). gB-Δfurin was
372 functional in cell-cell fusion assays and able to complement gB-negative PrV to levels
373 comparable to WT-gB (Fig. 10C). These data demonstrate that furin-cleavage of PrV gB is not
374 necessary for its function in cell-cell fusion and complementation. The observed fusion
375 deficiency of W187A and Y192A variants thus cannot be attributed to the reduced furin-
376 cleavage alone, but could still be caused by impaired trafficking and low surface expression.
377 Unlike HSV-1 gB, which is highly abundant at the cell surface, WT PrV gB exhibits rather low
378 surface expression. Only around 4% of WT PrV gB is targeted to the plasma membrane as
379 determined by FACS analysis (data not shown), making robust quantification complicated.

Next, the function of the mutated proteins during virus entry was tested in trans-complementation assay. RK13 cells were transfected with the different gB expression plasmids and infected one day later with a PrV mutant lacking the gB gene (PrV-ΔgB) (77). Cells and supernatant were harvested 24h p.i. and progeny viral titers were determined on RK13-gB cells (Fig. 9A). Cells transfected with expression plasmids for gBs which efficiently mediated cell-cell fusion also complemented the defect of PrV-ΔgB during entry comparable to WT gB. In contrast, no infectious progeny was derived from cells transfected with the empty vector ("mock"). Infectious progeny was also not produced after infection of cells transfected with the expression plasmid for W187A indicating that this gB mutant is not functional. Surprisingly, gB mutants Y192A, F275A, and F275Y which were unable to mediate cell-cell fusion supported production of a low titer of infectious virions (10^2 PFU/ml), while expression of Y276A resulted in titers of 10^4 PFU/ml, indicating that presence of other viral proteins might have partially compensated for the impairment in membrane binding and fusion.

DISCUSSION

Comparison with the available gB structures from other herpes viruses. The structural alignment of PrV gB with the homologous HSV-1, EBV and HCMV proteins demonstrates that the post-fusion conformation is well preserved, with the main difference residing in the positioning of domain IV relative to the rest of the protein (Fig. 2). The low-resolution structure obtained for the full-length HSV-1 gB in a conformation distinct from the post-fusion conformation localizes domain IV to the interior of the spike (30), implying that a large movement would occur during the conformational change. Insertion of a foot-and-mouth

disease virus (FMDV) epitope in PrV gB domain IV, right after the residue *Arg685*, resulted in high titers of neutralizing antibodies against FMDV (78), suggesting that at least some of the antigenic determinants on PrV gB domain IV are presented at the surface when the protein is expressed in its pre-fusion form. It is also possible, however, that the epitope is available because a fraction of gB at the virion surface may have adopted the post-fusion conformation.

Cholesterol dependence. HSV-1 gB binding to membranes was previously concluded to be cholesterol-dependent based on experiments using binary liposomes made of DOPC and CH (55). As we show in this study, the ability of PrV gB to bind to liposomes is not only influenced by its FL residues, but also by the lipid membrane composition. WT PrV gB ectodomains, as well as Y192F, Y267A and Y276F variants, showed increased binding to '4L' compared to '2L' liposomes, whose composition does not emulate well a real biological membrane (Fig. 9B). We show here that liposomes, either 2L or 4L, need to contain at least 40% CH for gB to bind (Fig. 3C), which is in agreement with 30-40% CH being present in plasma membrane and secretory vesicles (76), and with PrV entering cells via fusion with the plasma membrane. In case of herpesviruses that enter cells by endocytosis, the requirement for high CH concentration might also indicate that the fusion would occur within the internal compartments enriched in CH. A possible role for CH could be to fill the voids in the leaflet introduced by displacement of the bulkier head-groups of the other lipids upon insertion of the FLs.

Cholesterol has been shown previously to induce lipid curvature and promote formation of lipid stalks in fusion intermediates (25). While CH depletion was reported not to affect PrV attachment to cells, the virus was observed as stalled at the plasma membrane and entry was

424 significantly reduced (59). It was speculated that the particles might have been blocked due to
425 the inability to resolve the hemifusion intermediate in the absence of cholesterol, which is
426 contrary to our observation that CH is required for the initial insertion of FLs into the
427 membrane i.e. for an early event that must take place prior to reaching the hemifusion state.
428 HSV-1 gB full-length protein expressed on cells was shown to associate specifically with
429 CH- and SM-enriched lipid rafts (61), in which the two lipids are organized in the so-called
430 ordered lipid domains (Lo) (79). The borders between these Lo and the more fluid, disordered
431 membrane domains (Ld) were identified as the preferred sites for insertion of the HIV Env class
432 I fusion protein FP (80), presumably because they impose the least energy penalty for insertion
433 due to the line tension caused by the discontinuity between the domains. Desplanques *et al.*
434 had previously observed a significant fraction of PrV virions juxtaposed to the lipid raft marker
435 GM1 (59), which could, in the light of the Env insertion mode, indicate that PrV may use Lo-Ld
436 boundaries as sites of attachment as well. Although the FP of HIV Env is a short hydrophobic
437 sequence that has a free N-terminus, in contrast to the bipartite internal FLs of gB, it is
438 tempting to speculate that despite the different nature of the inserted segments, similar
439 energetic constraints might apply to membrane insertion of these divergent proteins. Further
440 experimental studies on herpesvirus gB are needed to test these hypotheses, and to establish if
441 CH is required for binding of herpesviruses to membranes, for membrane fusion or for both. It
442 is worth noting out that our EM data show an even distribution of the PrV gB ectodomains
443 bound to liposomes, opposing the idea of gB having preferred membrane insertion sites. This
444 could be due to the properties of the liposomes used for EM, which were made of 60% DOPC
445 and 40% CH, a binary mixture that would be expected to form the Lo phase only (81).

446

447 **Furin processing.** Proteolytic cleavage by cellular furin had been previously reported to be
448 dispensable for gB function in herpesviruses encoding cleavable gBs, as its absence did not have
449 an effect on viral replication or penetration kinetics, although smaller syncytia were detected
450 (82-86). A similar observation was made when gB was expressed in LoVo cells, which are
451 naturally deficient in furin, suggesting that PrV gB cleavage may play a role in cell-cell fusion
452 (84). Our data demonstrate that furin-cleavage of PrV gB was not required for its activity in cell-
453 cell fusion and virus trans-complementation assays used in this study (Fig. 10). The discrepancy
454 between our results regarding the gB-Δfurin variant function in cell-cell fusion and those
455 reported by Okazaki (84) could be due to the different cells types used for fusion.

456

457 **PrV gB FL variants in liposome binding and functional assays**. The liposome binding
458 experiments performed with the 15 recombinant gB ectodomain variants studied here allowed
459 the selection of a subset of variants to be followed up by studies in the context of the full-
460 length protein, both in cell-cell fusion and after incorporation into virus particles. The gB
461 ectodomains in interaction with liposomes provided snapshots of the protein already in the
462 post-fusion form, (Figs. 6A, 8B, 8C). The functional assays, on the other hand, illuminated the
463 function of full-length protein mutants expressed at the cell surface or incorporated into virus
464 particles in their pre-fusion state (Fig. 9A). This may explain certain discrepancies for instance
465 with variants that expressed well as recombinant ectodomains but that failed to be folded and
466 transported to the cell surface in cells. The selected variants of full-length gB were assessed for

their ability to mediate fusion in two functional assays: virus-free cell-cell fusion assay and trans-complementation of gB-negative PrV (18, 19, 21, 72).

To simplify comparisons with gB from other herpesviruses, we have numbered the FL residues from 1 to 14 (Fig. 5A). Our mutagenesis data are consistent with a model in which residues *Trp187 (*FL1-3), *Tyr192* (FL1-8) and *Tyr276* (FL2-10) form an aromatic surface compatible with insertion into the polar region of the membrane, establishing an 'interfacial rim' structure that would provide multiple interactions with the lipid head groups, while *Phe275* (FL2-9) would reach deeper into the hydrocarbon core (Fig. 11A). gB sequence conservation in alphaherpesviruses shows that residues with similar membrane-partitioning preferences are found at these four positions (supplemental material Fig. S1). Hydrophobic residues compatible with the insertion into the membrane core are present at FL2-9 (*Phe, Val, Leu, Trp*), while amphipathic side chains that would favor the interfacial region (*Tyr, His, Trp*) are found at positions FL1-3, FL1-8 and F2-10. This suggests that a common mode of gB insertion into membranes may have evolved within the alphaherpesvirus subfamily, although the residues interacting with lipids may not be identical. Charged residues such as *Arg* and *Glu* are present in the FLs of HSV-1 but not of PrV gB (Fig. 5A), highlighting intrinsic differences that exist despite potentially shared principles for insertion of aromatic and hydrophobic residues.

The FL2-9 position is always occupied with a hydrophobic side chain, such as *Phe275* in PrV gB. Mutation of the corresponding residue in HSV-1 gB (*Phe262*) to *Asp* or *Leu*, respectively, resulted in a poorly expressed protein and a protein that could mediate fusion at 70% of the level measured for the WT protein (52, 55). The tolerance for *Leu* (but not for *Asp*) in HSV-1 gB

and for *Trp* (but not for *Tyr*) in PrV gB indicates that FL2-9 has the potential to insert into the membrane core, i.e. deeper than the interfacial region.

Positions FL1-3 (*Trp187*), FL1-5 (*Gly189)* and FL1-8 (*Tyr192*) are occupied by the best conserved residues in FL1 of alphaherpesviruses (supplemental material Fig. S1, Fig. 12). FL1-5 *Gly* has already been shown to be important for function of HSV-1 gB (55), and was not tested here. Substitution of FL1-3 (*Trp*) of HSV-1 for a *Tyr* resulted in a protein that was 50% active in fusion (52). When the same residue was changed to *Phe* in PrV gB, the resulting ectodomain did not co-float with liposomes. It is possible that the FL1-3 position requires *Trp* because its indole ring may be involved in interactions with a specific lipid, and/or because its central location in between FL1-8 and FL2-10 might be important for the structural integrity and docking of the trio of rim residues into the membrane interface. HSV-1 gB variants containing a *Ser* and *Arg* at positions FL1-3 and FL1-8, respectively, were shown to be defective in fusion and in liposome-binding (55). These variants were subsequently crystallized, demonstrating that the mutations did not introduce any structural changes in FL1, and that the loss of binding to liposomes was solely due to the elimination of the hydrophobic side chains (87). While we anticipate that the same is true for the PrV gB ectodomains with mutations in FL1-3 and FL1-8, it is important to note that when expressed in cells as full-length proteins, W187A and Y192A accumulated in intracellular compartments and showed impaired processing (Fig. 8). We speculate that furin site in the misfolded gB variants may not be accessible for cleavage, giving rise to the observed decrease in the amount of cleaved protein. The possibility therefore remains that these two FL1 variants were not active in functional assays due to the altered cellular localization, even though the production of the ectodomains with the same mutations in insect cells led to

efficient protein secretion into the medium, suggesting that these residues are at least not important for correct folding of the post-fusion ectodomain.

The FL2-10 residue is predicted to insert into the interfacial region, and while PrV gB Y276F was functional, Y276A did not associate with liposomes and failed to mediate cell-cell fusion, although it unexpectedly partially rescued gB-null virus in the complementation assay. This result emphasizes distinct functional requirements for cell-cell fusion and viral entry processes, and that the two do not follow identical mechanisms. This is highlighted by the requirement for gD in PrV entry, but not for cell-cell spread (18, 88). The presence of other viral proteins during infection may compensate for the reduced membrane binding activity, and/or the protein may be present in higher density in the virion envelope than at the cell surface, favoring the fusion function.

FL2-1 is the most conserved FL2 residue in alphaherpesviruses, being *Tyr* in 75% of the sequences (supplemental material Fig. S1, Fig. 12). This residue was not mutagenized in HSV-1 gB, but was analyzed here for PrV gB, revealing to our surprise that changes to *Ala* or *Phe* had no effect. This suggests that *Tyr267* is not directly involved in interactions with liposomes, and is not essential for the protein function in fusion. Interestingly, Y267F bound indiscriminately to '2L' and '4L' liposomes, while Y267A was sensitive to the lipid composition and associated better with the '4L' liposomes. Membrane composition has been shown to influence binding of other viral fusion proteins of flaviviruses (89, 90), bunyaviruses (91), influenza virus (92) and HIV (93). In the latter case, the FP of gp41 was shown to adopt an α-helical or β-strand structure, depending on CH concentration, indicating alternative modes of insertion into membranes of the same protein.

532 Position FL2-11 is occupied by *Arg* in most alphaherpesviruses, and with *His* in PrV gB.
533 The substitution of this residue for *Ala* or larger *Trp* in PrV gB resulted in a functional protein
534 that associated with liposomes, indicating that this aromatic side chain is not important for
535 interactions with lipids. In contrast, *Arg* present at the same position in HSV-1 gB and in 26
536 other analyzed sequences (supplemental material Fig. S1), was implicated in binding to
537 liposomes, possibly by interacting with the negatively charged phosphate head-groups of
538 membrane lipids (55). The *His* and *Arg* side chains present at position FL2-11 obviously play
539 different roles in binding to lipids.
540
541 **Model of PrV gB interactions with lipids.** We show here that PrV gB residues *Trp187*, *Tyr192*,
542 *Gly274*, *Phe275* and *Tyr276* form a continuous, electrostatically neutral hydrophobic surface
543 (Fig. 7B) reminiscent of the hydrophobic patch reported for HSV-1 gB (55). EBV and HCMV gB
544 ectodomains used for crystallization had polar and charged residues inserted in place of the
545 hydrophobic WT FL residues, but similar hydrophobic patches at the base of the trimers are
546 observed when the WT residues are modeled back on the structure (data not shown). This
547 strongly suggests functional conservation of the areas involved in membrane interactions.
548 Closer inspection of the HCMV and EBV gB FL residues found at the positions identified as the
549 membrane contact sites in PrV gB reveals that two of the three rim positions, FL1-3 and FL2-10,
550 are occupied by *Tyr*, similar to gB of alphaherpesviruses, while *Thr* and *Ala* are found at FL1-8 in
551 HCMV and EBV gB, respectively (Fig. 11B, C). The *Tyr* residues at FL1-3 and FL2-10 are highly
552 conserved in beta- and gamma herpesviruses (data now shown), while FL1-8 is not. In addition,
553 the side chain of *Tyr*, found at neighboring FL1-10 in HCMV and at FL1-7 in HCMV and EBV gB,

554 could reach the plane in which FL1-3 and FL2-10 side chains insert, contributing to formation of
555 the interfacial rim. FL2-9, which according to our model inserts deeper, is *Leu* in HCMV and *Thr*
556 in EBV gB, while *Trp* is found at FL2-8 in both proteins. This *Trp* is strictly conserved within beta-
557 and partially within gamma-herpesviruses, while the latter have in addition a well-conserved
558 *Trp* inserted between FL2-5 and FL2-6 (designated as FL2-5*6 on Fig. 11B). There are also other
559 hydrophobic residues in the FLs on HCMV and EBV gB, whose side chains could insert into the
560 lipid bilayer (FL1-4, FL1-5, and FL1-6 in HCMV, and FL1-6, FL2-6 and FL2-7 in EBV gB; not shown
561 on Fig. 11B for clarity reasons). Thus, although they have more hydrophobic residues at the tips
562 of the FLs, our model suggests that beta- and gamma-herpesviruses gB interacts with the
563 membranes in a similar way as alpha-herpesvirus gB, with exposed hydrophobic residues in FL2
564 penetrating into the hydrocarbon core (FL2-9 and/or FL2-8 and/or FL2-5*6), while the rim
565 formed by residues from both FLs (FL1-3, FL1-7, FL2-10) would secure protein insertion into the
566 interface. The exact molecular mechanism through which this is achieved may vary, pointing to
567 differences between the herpesvirus subfamilies that might be related to the different host
568 cells and the specific composition of the target membranes.

569 **Materials and Methods**.

570 **Expression and purification of PrV gB ectodomain in insect cells for crystallization studies**

571 The synthetic gene encoding gB of Suid herpesvirus 1, Kaplan strain (GenBank number
572 AEM64049.1) was codon optimized for protein expression in *Drosophila* Schneider 2 (S2) cells
573 and purchased from Genscript. The gene segment coding the ectodomain (PrV gB residues 59-
574 756) was cloned into the expression vector pT350 (62), so that the ectodomain was flanked by
575 the *Drosophila* Bip secretion signal, driving efficient protein secretion (94) at the N-terminus,
576 and the enterokinase-cleavable double strep tag (sequence SRFESDDDDKAG WSHPQFEK
577 GGGSGGGSGGGS WSHPQFEK) at the C-terminus. Protein expression was induced by addition of
578 0.5mM $CuSO_4$, and the protein was harvested from the culture supernatant 7 days post-
579 induction (detailed protocol available in (63)). Standard protocols were applied to purify the
580 protein by affinity (Streptactin resin, IBA Technologies) and then by size exclusion
581 chromatography using 10mM Tris, 50mM NaCl pH 8 buffer and Superdex S200 column.
582 Extinction coefficient of 1.2 ml/mg for protein absorbance at 280nm was used for calculation of
583 protein concentration.

584

585 **Crystallization and structure determination of PrV gB ectodomain**

586 Purified PrV gB ectodomains were deglycosylated with endo-β-N-acetylglucosaminidase (Endo
587 D) from Streptococcus pneumoniae (95), by an overnight incubation of gB and Endo D in 10:1
588 ratio (weight: weight) in 50mM sodium-phosphate buffer pH 7.5 at 25°C. Reaction mixture was
589 then loaded onto Superdex S200 column to separate deglycosylated gB from Endo D, using

10mM Tris, 50mM NaCl pH 8 buffer. Fractions corresponding to gB were pooled, and the protein was concentrated to 9.2 mg/ml in 50kDa cut-off Vivaspin concentrator.

Crystals were grown by vapor diffusion in hanging drops in 0.1M Tris pH 8.5, 7% PEG 4,000, 0.6M LiCl, and then flash frozen in liquid nitrogen using 20% glycerol as the cryo-protectant. Data was collected at the ESRF synchrotron source ID29 beamline, and processed using XDS (96). Molecular replacement was done with Phaser (97) using HSV-1 gB structure (PDB 2GUM) as a search model. Structure was refined using BUSTER (98).

Electron microscopy

Samples for negative stain EM were prepared by mixing 0.5μM protein and 1mM liposomes as described in more detail in the 'liposome floatation assay' below. Liposomes were made of 60% DOPC and 40% CH. Staining was done with 2% uranyl-acetate, and images were collected on Tecnai G2 Spirit Biotwin microscope 5 (FEI, USA) operating at an accelerating voltage of 120 kV. Samples for cryo-EM analysis were made by incubating 4μM protein and 2mM liposomes. Cryo-fixation was done using Lacey grids using in EMGP (Leica, Austria). Data were recorded on Tecnai F20 operating at 200kv, equipped with a Falcon II direct detector (FEI, USA) and under low dose conditions.

Generation of expression constructs and production of PrV gB recombinant ectodomains in mammalian cells

The gene encoding PrV gB ectodomain residues 59-756, followed by a double strep tag, was cloned into pcDNA4 (Invitrogen™) expression vector using Gibson Assembly Master Mix® (New

612 England Biolabs). Quikchange mutagenesis was applied to introduce single point mutations in
613 the FLs, following the standard protocols (Agilent Technologies, QuikChange II site-directed
614 mutagenesis kit™). The presence of desired mutations was confirmed by DNA sequencing. The
615 expression constructs were transfected into Expi293F™ mammalian cells (Gibco) using
616 Expifectamine transfection agent, and as described in the manufacturer's manual. Cell
617 supernatants were collected 5 days post-transfection, and the protein was purified by affinity
618 chromatography on Streptactin resin (IBA Technologies) followed by SEC.
619
620 **Liposome floatation assay**
621 Lipids, DOPC (1,2-dioleoyl-sn-glycero-3-phosphocholine), DOPE (1,2-dioleoyl-sn-glycero-3-
622 phosphoethanolamine), SM (from bovine brain) and CH (from ovine wool), were purchased
623 from Avanti Polar Lipids. Liposomes were prepared by the freeze-thaw and extrusion method
624 (99), using 200nm membranes for extrusion. '2L' liposomes were made of 60% DOPC, 40% CH
625 (mol%), and '4L' liposomes of 20% DOPC, 20% DOPE, 20% SM and 40% CH (mol%).
626 Recombinant 0.5μM gB ectodomains were mixed with 1mM liposomes in PBS buffer in 100μl
627 volume, incubated overnight (12-15h) at 4°C and then at 37°C for 15 minutes (the overnight
628 incubation can be omitted, and was done for convenience reasons). OptiPrep medium (Axis-
629 Shield PoC AS, Oslo Norway) was used for density gradient preparation. Protein-liposome
630 samples were adjusted to the volume of 300μl by addition of 30μl of PBS and 170μl of 60%
631 OptiPrep (final Optiprep concetration 36%), and deposited with a syringe on the bottom of the
632 ultracentrifuge tube already containing 4.5ml of 20% Optiprep solution in PBS. 200μl of PBS was
633 added to the top, and the samples were centrifuged for 1h at 40,000 x g and 4°C, in SWTi 55

swinging bucket rotor in Beckman Coulter ultracentrifuge. The 5ml gradients were fractionated into 2 x 400µl fractions (the first one representing the 'top' fraction), 3 x 1.2ml and 1 x 600µl ('bottom') fraction. 30µl aliquots of the top and bottom fractions were analyzed on SDS-PAGE 4-20% gradient gels (GenScript), and Western blotting to detected the double strep tag on gB was done with the Streptactin-HRP conjugate (IBA Technologies) following the manufacturer's instructions.

Viruses and cells. Rabbit kidney (RK13) and RK13-gB cells were grown in Dulbecco's modified Eagle's minimum essential medium (MEM) supplemented with 10% fetal calf serum at 37°C and 5 % CO_2. PrV mutant lacking gB (PrV-ΔgB) (77), which was derived from PrV strain Kaplan (PrV-Ka), was propagated in RK13-gB cells.

Expression plasmids for cell-cell fusion assay. Generation of expression plasmids for PrV-Kaplan (PrV-Ka) gB, gH, and gL has been described previously (71). Expression plasmid pcDNA-gB^{Ka} containing the gB open reading frame (ORF UL27) was used for site-directed mutagenesis (QuikChange II XL kit, Agilent) with the complementary pair of oligonucleotide primers. Correct mutagenesis was verified by sequencing.

***In vitro* cell-cell fusion assays.** Fusion activity of the different gB-mutants was analyzed after transient transfection of RK13 cells as described recently (73). Briefly, approximately 1.8×10^5 RK13 cells per well were seeded onto 24-well cell culture plates. On the following day, cells were transfected with 200 ng each of expression plasmids for EGFP (pEGFP-N1; Clontech), and

for PrV glycoproteins gB^{Ka} or mutant gB, gL^{Ka} and gH^{Ka} (21, 71, 100) in 100 µl Opti-MEM using 1 µl Lipofectamine 2000 (Thermo Fisher Scientific). Empty vector (pcDNA3) served as negative control. The mixture was incubated for 20 min at room temperature and added to the cells. After 3 hours, cells were washed with PBS and incubated in MEM supplemented with 2% FCS for another 24 h at 37°C. Thereafter, cells were fixed with 3% paraformaldehyde (PFA). Syncytia formation was analyzed using an Eclipse Ti-S fluorescence microscope and the NIS-Elements Imaging Software (Nikon). Total fusion activity was determined by multiplication of the area of cells with three or more nuclei with the number of syncytia within 10 fields of view (5.5 mm^2 each). The experiment was repeated three times and average percent values of positive control transfections as well as standard deviations were calculated.

Trans-complementation assay. Function of the different gB mutants in virus entry was determined by trans-complementation of PrV-ΔgB (77). Approximately 1.8×10^5 RK13 cells per well were seeded onto 24-well cell culture plates. On the following day, cells were transfected with 200 ng of the corresponding gB-expression plasmid as described above. One day post transfection cells were infected with phenotypically gB-complemented PrV-ΔgB at an MOI of 3, and consecutively incubated on ice for 1 h and at 37°C for 1 h. Subsequently, the inoculum was removed, non-penetrated virus was inactivated by low-pH treatment (101), and 1 ml fresh medium was added. After 24h at 37°C, the cells were harvested together with the supernatants and lysed by freeze-thawing (-80°C and 37°C). Progeny virus titers were determined on PrV gB-expressing cells (RK13-gB) (77). Shown are the mean values of three independent experiments with the corresponding standard deviation.

678

679 **Indirect immunofluorescence tests.** To test for subcellular localization of the mutated proteins,
680 RK13 cells were transfected with the gB expression plasmids as described above. After 24 h,
681 cells were fixed with 3% paraformaldehyde (PFA) for 20 min and permeabilized in PBS
682 containing 0,1 % Triton X-100 for 10 min at room temperature. Subsequently, cells were
683 incubated with a rabbit antiserum specific for PrV gB (102), which was diluted 1:1000 in PBS.
684 After 1 hour at room temperature, bound antibody was detected with Alexa 488-conjugated
685 goat anti-rabbit antibodies (1:1000 in PBS) (Invitrogen). After each step, cells were washed
686 repeatedly with PBS. Green fluorescence was excited at 488 nm, and recorded with a laser
687 scanning confocal microscope (SP5; Leica, Mannheim, Germany).

688

689 **Western blot analyses.** RK13 cells were harvested 24 h after transfection with the different gB
690 expression plasmids, as described above. Cells were lysed and protein samples were separated
691 by sodium dodecyl sulfate 10% polyacrylamide gel electrophoresis (SDS-PAGE) and transferred
692 to a nitrocellulose membrane. The membrane was incubated with a monoclonal gB-antibody
693 (C15-b1 at 1:500 dilution) (102, 103). Binding of peroxidase-conjugated secondary antibody
694 (Jackson ImmunoResearch) was detected with Clarity™ Western ECL substrate (Bio-Rad) and
695 recorded by VersaDoc 4000 MP imager (Bio-Rad).

696

697 **ACKNOWLEDGMENTS.**

698 Work done by M.B., D.B., M.C.V., P.G.C. and F.A.R. was supported by Institut Pasteur and CNRS
699 recurrent funding, and the Pasteur-Weizmann / Servier International Prize (F.A.R., 2015). We

700 acknowledge assistance of the Core facilities for crystallization and microscopy at Institut
701 Pasteur, and also thank M. Nilges and the Equipex CACSICE for providing the Falcon II direct
702 detector, and we thank the European Synchrotron Radiation Facility for help during data
703 collection. Work done by M.V., B.K., and T.C.M. was supported by DFG, grant Me 854/11-2.

REFERENCES

1. **Pellet PE, Roizman B.** 2014. Herpesviridae, p 1802-1822. *In* Knipe DM, Howley PM (ed), Fields Virology, 6th ed, vol 2. Lippincott Williams & Wilkins, New York.
2. **Mettenleiter TC.** 1996. Immunobiology of pseudorabies (Aujeszky's disease). Vet Immunol Immunopathol **54:**221-229.
3. **Pomeranz LE, Reynolds AE, Hengartner CJ.** 2005. Molecular biology of pseudorabies virus: impact on neurovirology and veterinary medicine. Microbiol Mol Biol Rev **69:**462-500.
4. **Eisenberg RJ, Atanasiu D, Cairns TM, Gallagher JR, Krummenacher C, Cohen GH.** 2012. Herpes virus fusion and entry: a story with many characters. Viruses **4:**800-832.
5. **Nicola AV.** 2016. Herpesvirus Entry into Host Cells Mediated by Endosomal Low pH. Traffic **17:**965-975.
6. **Li A, Lu G, Qi J, Wu L, Tian K, Luo T, Shi Y, Yan J, Gao GF.** 2017. Structural basis of nectin-1 recognition by pseudorabies virus glycoprotein D. PLoS Pathog **13:**e1006314.
7. **Spear PG.** 2004. Herpes simplex virus: receptors and ligands for cell entry. Cell Microbiol **6:**401-410.
8. **Vanarsdall AL, Chase MC, Johnson DC.** 2011. Human cytomegalovirus glycoprotein gO complexes with gH/gL, promoting interference with viral entry into human fibroblasts but not entry into epithelial cells. Journal of virology **85:**11638-11645.
9. **Mullen MM, Haan KM, Longnecker R, Jardetzky TS.** 2002. Structure of the Epstein-Barr virus gp42 protein bound to the MHC class II receptor HLA-DR1. Mol Cell **9:**375-385.
10. **Krummenacher C, Carfi A, Eisenberg RJ, Cohen GH.** 2013. Entry of herpesviruses into cells: the enigma variations. Adv Exp Med Biol **790:**178-195.
11. **Sathiyamoorthy K, Chen J, Longnecker R, Jardetzky TS.** 2017. The COMPLEXity in herpesvirus entry. Curr Opin Virol **24:**97-104.
12. **Agelidis AM, Shukla D.** 2015. Cell entry mechanisms of HSV: what we have learned in recent years. Future Virol **10:**1145-1154.
13. **Di Giovine P, Settembre EC, Bhargava AK, Luftig MA, Lou H, Cohen GH, Eisenberg RJ, Krummenacher C, Carfi A.** 2011. Structure of herpes simplex virus glycoprotein D bound to the human receptor nectin-1. PLoS Pathog **7:**e1002277.
14. **Lazear E, Whitbeck JC, Zuo Y, Carfi A, Cohen GH, Eisenberg RJ, Krummenacher C.** 2014. Induction of conformational changes at the N-terminus of herpes simplex virus glycoprotein D upon binding to HVEM and nectin-1. Virology **448:**185-195.
15. **Gianni T, Amasio M, Campadelli-Fiume G.** 2009. Herpes simplex virus gD forms distinct complexes with fusion executors gB and gH/gL in part through the C-terminal profusion domain. J Biol Chem **284:**17370-17382.
16. **Atanasiu D, Saw WT, Cohen GH, Eisenberg RJ.** 2010. Cascade of events governing cell-cell fusion induced by herpes simplex virus glycoproteins gD, gH/gL, and gB. J Virol **84:**12292-12299.
17. **Schmidt J, Klupp BG, Karger A, Mettenleiter TC.** 1997. Adaptability in herpesviruses: glycoprotein D-independent infectivity of pseudorabies virus. Journal of virology **71:**17-24.

18. **Rauh I, Mettenleiter TC.** 1991. Pseudorabies virus glycoproteins gII and gp50 are essential for virus penetration. J Virol **65:**5348-5356.
19. **Peeters B, de Wind N, Broer R, Gielkens A, Moormann R.** 1992. Glycoprotein H of pseudorabies virus is essential for entry and cell-to-cell spread of the virus. J Virol **66:**3888-3892.
20. **Klupp BG, Fuchs W, Weiland E, Mettenleiter TC.** 1997. Pseudorabies virus glycoprotein L is necessary for virus infectivity but dispensable for virion localization of glycoprotein H. J Virol **71:**7687-7695.
21. **Schröter C, Vallbracht M, Altenschmidt J, Kargoll S, Fuchs W, Klupp BG, Mettenleiter TC.** 2016. Mutations in Pseudorabies Virus Glycoproteins gB, gD, and gH Functionally Compensate for the Absence of gL. J Virol **90:**2264-2272.
22. **Roche S, Bressanelli S, Rey FA, Gaudin Y.** 2006. Crystal structure of the low-pH form of the vesicular stomatitis virus glycoprotein G. Science **313:**187-191.
23. **Kadlec J, Loureiro S, Abrescia NG, Stuart DI, Jones IM.** 2008. The postfusion structure of baculovirus gp64 supports a unified view of viral fusion machines. Nat Struct Mol Biol **15:**1024-1030.
24. **Harrison SC.** 2015. Viral membrane fusion. Virology **479-480:**498-507.
25. **Chernomordik LV, Kozlov MM.** 2008. Mechanics of membrane fusion. Nat Struct Mol Biol **15:**675-683.
26. **Heldwein EE, Lou H, Bender FC, Cohen GH, Eisenberg RJ, Harrison SC.** 2006. Crystal structure of glycoprotein B from herpes simplex virus 1. Science **313:**217-220.
27. **Backovic M, Longnecker R, Jardetzky TS.** 2009. Structure of a trimeric variant of the Epstein-Barr virus glycoprotein B. Proc Natl Acad Sci U S A **106:**2880-2885.
28. **Chandramouli S, Ciferri C, Nikitin PA, Calo S, Gerrein R, Balabanis K, Monroe J, Hebner C, Lilja AE, Settembre EC, Carfi A.** 2015. Structure of HCMV glycoprotein B in the postfusion conformation bound to a neutralizing human antibody. Nat Commun **6:**8176.
29. **Burke HG, Heldwein EE.** 2015. Crystal Structure of the Human Cytomegalovirus Glycoprotein B. PLoS Pathog **11:**e1005227.
30. **Zeev-Ben-Mordehai T, Vasishtan D, Hernandez Duran A, Vollmer B, White P, Prasad Pandurangan A, Siebert CA, Topf M, Grunewald K.** 2016. Two distinct trimeric conformations of natively membrane-anchored full-length herpes simplex virus 1 glycoprotein B. Proc Natl Acad Sci U S A **113:**4176-4181.
31. **Roche S, Rey FA, Gaudin Y, Bressanelli S.** 2007. Structure of the prefusion form of the vesicular stomatitis virus glycoprotein G. Science **315:**843-848.
32. **Gallagher JR, Atanasiu D, Saw WT, Paradisgarten MJ, Whitbeck JC, Eisenberg RJ, Cohen GH.** 2014. Functional fluorescent protein insertions in herpes simplex virus gB report on gB conformation before and after execution of membrane fusion. PLoS Pathog **10:**e1004373.
33. **Chowdary TK, Cairns TM, Atanasiu D, Cohen GH, Eisenberg RJ, Heldwein EE.** 2010. Crystal structure of the conserved herpesvirus fusion regulator complex gH-gL. Nat Struct Mol Biol **17:**882-888.
34. **Matsuura H, Kirschner AN, Longnecker R, Jardetzky TS.** 2010. Crystal structure of the Epstein-Barr virus (EBV) glycoprotein H/glycoprotein L (gH/gL) complex. Proc Natl Acad Sci U S A **107:**22641-22646.

35. **Xing Y, Oliver SL, Nguyen T, Ciferri C, Nandi A, Hickman J, Giovani C, Yang E, Palladino G, Grose C, Uematsu Y, Lilja AE, Arvin AM, Carfi A.** 2015. A site of varicella-zoster virus vulnerability identified by structural studies of neutralizing antibodies bound to the glycoprotein complex gHgL. Proc Natl Acad Sci U S A **112:**6056-6061.
36. **Backovic M, DuBois RM, Cockburn JJ, Sharff AJ, Vaney MC, Granzow H, Klupp BG, Bricogne G, Mettenleiter TC, Rey FA.** 2010. Structure of a core fragment of glycoprotein H from pseudorabies virus in complex with antibody. Proc Natl Acad Sci U S A **107:**22635-22640.
37. **Heldwein EE.** 2016. gH/gL supercomplexes at early stages of herpesvirus entry. Curr Opin Virol **18:**1-8.
38. **Atanasiu D, Saw WT, Cohen GH, Eisenberg RJ.** 2010. Cascade of events governing cell-cell fusion induced by herpes simplex virus glycoproteins gD, gH/gL, and gB. Journal of virology **84:**12292-12299.
39. **White JM, Delos SE, Brecher M, Schornberg K.** 2008. Structures and mechanisms of viral membrane fusion proteins: multiple variations on a common theme. Crit Rev Biochem Mol Biol **43:**189-219.
40. **Ito H, Watanabe S, Sanchez A, Whitt MA, Kawaoka Y.** 1999. Mutational analysis of the putative fusion domain of Ebola virus glycoprotein. J Virol **73:**8907-8912.
41. **Apellaniz B, Huarte N, Largo E, Nieva JL.** 2014. The three lives of viral fusion peptides. Chem Phys Lipids **181:**40-55.
42. **Bressanelli S, Stiasny K, Allison SL, Stura EA, Duquerroy S, Lescar J, Heinz FX, Rey FA.** 2004. Structure of a flavivirus envelope glycoprotein in its low-pH-induced membrane fusion conformation. Embo J **23:**728-738.
43. **Voss JE, Vaney MC, Duquerroy S, Vonrhein C, Girard-Blanc C, Crublet E, Thompson A, Bricogne G, Rey FA.** 2010. Glycoprotein organization of Chikungunya virus particles revealed by X-ray crystallography. Nature **468:**709-712.
44. **DuBois RM, Vaney MC, Tortorici MA, Kurdi RA, Barba-Spaeth G, Krey T, Rey FA.** 2013. Functional and evolutionary insight from the crystal structure of rubella virus protein E1. Nature **493:**552-556.
45. **Dessau M, Modis Y.** 2013. Crystal structure of glycoprotein C from Rift Valley fever virus. Proc Natl Acad Sci U S A **110:**1696-1701.
46. **Guardado-Calvo P, Bignon EA, Stettner E, Jeffers SA, Perez-Vargas J, Pehau-Arnaudet G, Tortorici MA, Jestin JL, England P, Tischler ND, Rey FA.** 2016. Mechanistic Insight into Bunyavirus-Induced Membrane Fusion from Structure-Function Analyses of the Hantavirus Envelope Glycoprotein Gc. PLoS Pathog **12:**e1005813.
47. **Sun X, Belouzard S, Whittaker GR.** 2008. Molecular architecture of the bipartite fusion loops of vesicular stomatitis virus glycoprotein G, a class III viral fusion protein. J Biol Chem **283:**6418-6427.
48. **Baquero E, Albertini AA, Gaudin Y.** 2015. Recent mechanistic and structural insights on class III viral fusion glycoproteins. Curr Opin Struct Biol **33:**52-60.
49. **Backovic M, Leser GP, Lamb RA, Longnecker R, Jardetzky TS.** 2007. Characterization of EBV gB indicates properties of both class I and class II viral fusion proteins. Virology **368:**102-113.

50. **Sharma S, Wisner TW, Johnson DC, Heldwein EE.** 2013. HCMV gB shares structural and functional properties with gB proteins from other herpesviruses. Virology **435:**239-249.
51. **Backovic M, Jardetzky TS, Longnecker R.** 2007. Hydrophobic residues that form putative fusion loops of Epstein-Barr virus glycoprotein B are critical for fusion activity. J Virol **81:**9596-9600.
52. **Hannah BP, Heldwein EE, Bender FC, Cohen GH, Eisenberg RJ.** 2007. Mutational evidence of internal fusion loops in herpes simplex virus glycoprotein B. J Virol **81:**4858-4865.
53. **Lin E, Spear PG.** 2007. Random linker-insertion mutagenesis to identify functional domains of herpes simplex virus type 1 glycoprotein B. Proc Natl Acad Sci U S A **104:**13140-13145.
54. **Atanasiu D, Saw WT, Gallagher JR, Hannah BP, Matsuda Z, Whitbeck JC, Cohen GH, Eisenberg RJ.** 2013. Dual split protein-based fusion assay reveals that mutations to herpes simplex virus (HSV) glycoprotein gB alter the kinetics of cell-cell fusion induced by HSV entry glycoproteins. J Virol **87:**11332-11345.
55. **Hannah BP, Cairns TM, Bender FC, Whitbeck JC, Lou H, Eisenberg RJ, Cohen GH.** 2009. Herpes simplex virus glycoprotein B associates with target membranes via its fusion loops. J Virol **83:**6825-6836.
56. **Maurer UE, Zeev-Ben-Mordehai T, Pandurangan AP, Cairns TM, Hannah BP, Whitbeck JC, Eisenberg RJ, Cohen GH, Topf M, Huiskonen JT, Grunewald K.** 2013. The structure of herpesvirus fusion glycoprotein B-bilayer complex reveals the protein-membrane and lateral protein-protein interaction. Structure **21:**1396-1405.
57. **Yang ST, Kreutzberger AJ, Lee J, Kiessling V, Tamm LK.** 2016. The role of cholesterol in membrane fusion. Chem Phys Lipids **199:**136-143.
58. **Ren X, Yin J, Li G, Herrler G.** 2011. Cholesterol dependence of pseudorabies herpesvirus entry. Curr Microbiol **62:**261-266.
59. **Desplanques AS, Nauwynck HJ, Vercauteren D, Geens T, Favoreel HW.** 2008. Plasma membrane cholesterol is required for efficient pseudorabies virus entry. Virology **376:**339-345.
60. **Wudiri GA, Pritchard SM, Li H, Liu J, Aguilar HC, Gilk SD, Nicola AV.** 2014. Molecular requirement for sterols in herpes simplex virus entry and infectivity. J Virol **88:**13918-13922.
61. **Bender FC, Whitbeck JC, Ponce de Leon M, Lou H, Eisenberg RJ, Cohen GH.** 2003. Specific association of glycoprotein B with lipid rafts during herpes simplex virus entry. J Virol **77:**9542-9552.
62. **Krey T, d'Alayer J, Kikuti CM, Saulnier A, Damier-Piolle L, Petitpas I, Johansson DX, Tawar RG, Baron B, Robert B, England P, Persson MA, Martin A, Rey FA.** 2010. The disulfide bonds in glycoprotein E2 of hepatitis C virus reveal the tertiary organization of the molecule. PLoS Pathog **6:**e1000762.
63. **Backovic M, Krey T.** 2016. Stable Drosophila Cell Lines: An Alternative Approach to Exogenous Protein Expression. Methods Mol Biol **1350:**349-358.
64. **Culp JS, Johansen H, Hellmig B, Beck J, Matthews TJ, Delers A, Rosenberg M.** 1991. Regulated expression allows high level production and secretion of HIV-1 gp120 envelope glycoprotein in Drosophila Schneider cells. Biotechnology (N Y) **9:**173-177.

65. **Gianni T, Fato R, Bergamini C, Lenaz G, Campadelli-Fiume G.** 2006. Hydrophobic alpha-helices 1 and 2 of herpes simplex virus gH interact with lipids, and their mimetic peptides enhance virus infection and fusion. Journal of virology **80:**8190-8198.
66. **Sugihara K, Chami M, Derenyi I, Voros J, Zambelli T.** 2012. Directed self-assembly of lipid nanotubes from inverted hexagonal structures. ACS Nano **6:**6626-6632.
67. **Wimley WC, White SH.** 1996. Experimentally determined hydrophobicity scale for proteins at membrane interfaces. Nat Struct Biol **3:**842-848.
68. **MacCallum JL, Bennett WF, Tieleman DP.** 2008. Distribution of amino acids in a lipid bilayer from computer simulations. Biophys J **94:**3393-3404.
69. **Yau WM, Wimley WC, Gawrisch K, White SH.** 1998. The preference of tryptophan for membrane interfaces. Biochemistry **37:**14713-14718.
70. **White SH, Wimley WC.** 1999. Membrane protein folding and stability: physical principles. Annu Rev Biophys Biomol Struct **28:**319-365.
71. **Klupp BG, Nixdorf R, Mettenleiter TC.** 2000. Pseudorabies virus glycoprotein M inhibits membrane fusion. J Virol **74:**6760-6768.
72. **Turner A, Bruun B, Minson T, Browne H.** 1998. Glycoproteins gB, gD, and gHgL of herpes simplex virus type 1 are necessary and sufficient to mediate membrane fusion in a Cos cell transfection system. J Virol **72:**873-875.
73. **Vallbracht M, Schröter, C., Klupp, B. G. and Mettenleiter, T. C. .** 2017. Transient Transfection-based Fusion Assay for Viral Proteins. Bio-protocol **7**.
74. **Dodge JT, Phillips GB.** 1967. Composition of phospholipids and of phospholipid fatty acids and aldehydes in human red cells. J Lipid Res **8:**667-675.
75. **Virtanen JA, Cheng KH, Somerharju P.** 1998. Phospholipid composition of the mammalian red cell membrane can be rationalized by a superlattice model. Proc Natl Acad Sci U S A **95:**4964-4969.
76. **Kalvodova L, Sampaio JL, Cordo S, Ejsing CS, Shevchenko A, Simons K.** 2009. The lipidomes of vesicular stomatitis virus, semliki forest virus, and the host plasma membrane analyzed by quantitative shotgun mass spectrometry. J Virol **83:**7996-8003.
77. **Nixdorf R, Klupp BG, Karger A, Mettenleiter TC.** 2000. Effects of truncation of the carboxy terminus of pseudorabies virus glycoprotein B on infectivity. J Virol **74:**7137-7145.
78. **Dory D, Remond M, Beven V, Cariolet R, Backovic M, Zientara S, Jestin A.** 2009. Pseudorabies virus glycoprotein B can be used to carry foot and mouth disease antigens in DNA vaccination of pigs. Antiviral Res **81:**217-225.
79. **Rog T, Vattulainen I.** 2014. Cholesterol, sphingolipids, and glycolipids: what do we know about their role in raft-like membranes? Chem Phys Lipids **184:**82-104.
80. **Yang ST, Kiessling V, Tamm LK.** 2016. Line tension at lipid phase boundaries as driving force for HIV fusion peptide-mediated fusion. Nat Commun **7:**11401.
81. **Feigenson GW.** 2006. Phase behavior of lipid mixtures. Nat Chem Biol **2:**560-563.
82. **Oliver SL, Sommer M, Zerboni L, Rajamani J, Grose C, Arvin AM.** 2009. Mutagenesis of varicella-zoster virus glycoprotein B: putative fusion loop residues are essential for viral replication, and the furin cleavage motif contributes to pathogenesis in skin tissue in vivo. J Virol **83:**7495-7506.

83. **Sorem J, Longnecker R.** 2009. Cleavage of Epstein-Barr virus glycoprotein B is required for full function in cell-cell fusion with both epithelial and B cells. J Gen Virol **90:**591-595.
84. **Okazaki K.** 2007. Proteolytic cleavage of glycoprotein B is dispensable for in vitro replication, but required for syncytium formation of pseudorabies virus. J Gen Virol **88:**1859-1865.
85. **Strive T, Borst E, Messerle M, Radsak K.** 2002. Proteolytic processing of human cytomegalovirus glycoprotein B is dispensable for viral growth in culture. J Virol **76:**1252-1264.
86. **Kopp A, Blewett E, Misra V, Mettenleiter TC.** 1994. Proteolytic cleavage of bovine herpesvirus 1 (BHV-1) glycoprotein gB is not necessary for its function in BHV-1 or pseudorabies virus. J Virol **68:**1667-1674.
87. **Stampfer SD, Lou H, Cohen GH, Eisenberg RJ, Heldwein EE.** 2010. Structural basis of local, pH-dependent conformational changes in glycoprotein B from herpes simplex virus type 1. J Virol **84:**12924-12933.
88. **Peeters B, de Wind N, Hooisma M, Wagenaar F, Gielkens A, Moormann R.** 1992. Pseudorabies virus envelope glycoproteins gp50 and gII are essential for virus penetration, but only gII is involved in membrane fusion. J Virol **66:**894-905.
89. **Stiasny K, Koessl C, Heinz FX.** 2003. Involvement of lipids in different steps of the flavivirus fusion mechanism. J Virol **77:**7856-7862.
90. **Zaitseva E, Yang ST, Melikov K, Pourmal S, Chernomordik LV.** 2010. Dengue virus ensures its fusion in late endosomes using compartment-specific lipids. PLoS Pathog **6:**e1001131.
91. **Guardado-Calvo P, Rey FA.** 2017. The Envelope Proteins of the Bunyavirales. Adv Virus Res **98:**83-118.
92. **Domanska MK, Wrona D, Kasson PM.** 2013. Multiphasic effects of cholesterol on influenza fusion kinetics reflect multiple mechanistic roles. Biophys J **105:**1383-1387.
93. **Lai AL, Moorthy AE, Li Y, Tamm LK.** 2012. Fusion activity of HIV gp41 fusion domain is related to its secondary structure and depth of membrane insertion in a cholesterol-dependent fashion. J Mol Biol **418:**3-15.
94. **Kirkpatrick RB, Ganguly S, Angelichio M, Griego S, Shatzman A, Silverman C, Rosenberg M.** 1995. Heavy chain dimers as well as complete antibodies are efficiently formed and secreted from Drosophila via a BiP-mediated pathway. J Biol Chem **270:**19800-19805.
95. **Fan SQ, Huang W, Wang LX.** 2012. Remarkable transglycosylation activity of glycosynthase mutants of endo-D, an endo-beta-N-acetylglucosaminidase from Streptococcus pneumoniae. J Biol Chem **287:**11272-11281.
96. **Kabsch W.** 2010. XDS. Acta Crystallogr D Biol Crystallogr **66:**125-132.
97. **McCoy AJ, Grosse-Kunstleve RW, Adams PD, Winn MD, Storoni LC, Read RJ.** 2007. Phaser crystallographic software. J Appl Crystallogr **40:**658-674.
98. **Bricogne G, Blanc E, Brandl M, Flensburg C, Keller P, Paciorek W, Roversi P, Smart OS, Vonrhein C, Womack TO.** 2009. BUSTER, v2.8.0. Global Phasing Ltd., Cambridge, United Kingdom.
99. **Castile JD, Taylor KM.** 1999. Factors affecting the size distribution of liposomes produced by freeze-thaw extrusion. Int J Pharm **188:**87-95.

100. **Böhm SW, Eckroth E, Backovic M, Klupp BG, Rey FA, Mettenleiter TC, Fuchs W.** 2015. Structure-based functional analyses of domains II and III of pseudorabies virus glycoprotein H. J Virol **89:**1364-1376.
101. **Mettenleiter TC.** 1989. Glycoprotein gIII deletion mutants of pseudorabies virus are impaired in virus entry. Virology **171:**623-625.
102. **Kopp M, Granzow H, Fuchs W, Klupp BG, Mundt E, Karger A, Mettenleiter TC.** 2003. The pseudorabies virus UL11 protein is a virion component involved in secondary envelopment in the cytoplasm. J Virol **77:**5339-5351.
103. **Pavlova SP, Veits J, Keil GM, Mettenleiter TC, Fuchs W.** 2009. Protection of chickens against H5N1 highly pathogenic avian influenza virus infection by live vaccination with infectious laryngotracheitis virus recombinants expressing H5 hemagglutinin and N1 neuraminidase. Vaccine **27:**773-785.
104. **DeLano WL.** 2002. The PyMOL Molecular Graphics System, DeLano Scientific, San Carlos, CA, USA.
105. **Eisenberg D, Schwarz E, Komaromy M, Wall R.** 1984. Analysis of membrane and surface protein sequences with the hydrophobic moment plot. J Mol Biol **179:**125-142.
106. **Baker NA, Sept D, Joseph S, Holst MJ, McCammon JA.** 2001. Electrostatics of nanosystems: application to microtubules and the ribosome. Proc Natl Acad Sci U S A **98:**10037-10041.
107. **Hasegawa H, Holm L.** 2009. Advances and pitfalls of protein structural alignment. Curr Opin Struct Biol **19:**341-348.
108. **Sievers F, Wilm A, Dineen D, Gibson TJ, Karplus K, Li W, Lopez R, McWilliam H, Remmert M, Soding J, Thompson JD, Higgins DG.** 2011. Fast, scalable generation of high-quality protein multiple sequence alignments using Clustal Omega. Mol Syst Biol **7:**539.
109. **Gouet P, Courcelle E, Stuart DI, Metoz F.** 1999. ESPript: analysis of multiple sequence alignments in PostScript. Bioinformatics **15:**305-308.

991 **FIGURE LEGENDS AND TABLES.**

992 **Figure 1. PrV gB ectodomain structure. A) Schematic representation of the PrV gB expression**
993 **construct.** The PrV gB signal peptide (residues 1-58) was replaced by the *Drosophila* BiP
994 secretion signal, which was cleaved off and not part of the secreted protein. The secreted PrV
995 gB ectodomain used for crystallization contains residues 59-756, followed by a double strep tag
996 (DST). Regions forming the five gB domains are labeled with Roman numbers I to V below the
997 bar, and are colored as follows: domain I (blue), domain II (green), domain III (yellow), domain
998 IV (orange) and domain V (red). Two linker regions (residues 147-154 and 493-528) are shown
999 in grey. Dashed lines mark the regions that were unresolved in the gB structure. Location of the
1000 furin cleavage site ('RRARR' residues 501-505) is indicated. **B) SDS-PAGE analysis of the**
1001 **recombinant PrV gB.** Coomassie-blue stained 4-20% SDS-PAGE gel showing purified PrV gB
1002 ectodomain under non-reducing (lanes 1 and 2), and reducing (lanes 3 and 4) conditions.
1003 Samples in lanes 2 and 4 were treated with Endo D. The N-terminal and C-terminal fragments,
1004 generated by furin cleavage, are labelled as gB^b and gB^c, and the small fraction of uncleaved gB
1005 is marked as gB^a. **C) Structure of the PrV gB monomer**. The molecule is colored starting from
1006 blue (N-terminus) to red (C-terminus). The location of the N- and C-termini is indicated with the
1007 letters 'N' and 'C', and domains are labeled with Roman numbers I to V. The C-terminus is
1008 followed by the 50-residue long membrane-proximal region (MPR), not present in the
1009 expression construct, leading to the transmembrane anchor; the anticipated location of the
1010 membrane is indicated with the arrow. Fusion loops presented by domain I are marked with the
1011 star symbol (*) and 'FL'. The extra N-terminal residues that were resolved for the first time in
1012 this structure form a strand labeled as β1. The linker connecting domains II and III, which is not

visible in our structure, is plotted as a yellow dotted line to indicate the putative location of the furin cleavage site (orange star). The location of the glycosylation site *Asn264*, to which a single NAG residue is attached, is indicated with the yellow star. **D) Structure of the PrV gB trimer.** The same coloring for the protomers as in (C) applies. Ribbon and molecular surface representations are shown. The N- and C-termini of the same protomer represented in (B) are labeled with 'N' and 'C', respectively. Strand β29 that runs in anti-parallel direction to strand β1 is indicated (domain IV). PyMOL was used to create structures shown in panels (C) and (D) (104).

Figure 2. Structural comparison of gB ectodomains. PrV gB ectodomain structure, shown in grey cartoon representation, was superposed with those of HSV-1 (PDB 2GUM; light blue), CMV (PDB 5C6T; green) and EBV gB (PDB 3FVC; purple), using the residue range that corresponds to domains I and II (residues 167-458, 154-473, 89-388 and 133-415) of PrV, HSV-1, CMV, and EBV gB, respectively). The alignment was done by superposing domains I and II to highlight the disposition of the top, domain IV, which is not as obvious when the superposition is applied to the entire molecule. The alignments were done in PyMol (104). Domains are labeled with Roman numbers. Each superposition is shown in two orientations, looking at the monomer from the front (upper panel) and at domain IV from the top of the spike (lower panel). Red pentagon symbol is placed in the same loop of PrV gB to serve as a reference point for the movement of the superposed domain IV, the direction of which is indicated with the black arrow.

1035 **Figure 3. WT PrV gB ectodomains interactions with liposomes. A) WT gB ectodomains bind to**
1036 **the DOPC-CH liposomes.** Presence of liposomes ('L') and protein is indicated with + and – signs
1037 on the top. Aliquots of the top ('t') i.e. liposome, and bottom ('b') i.e. unbound protein,
1038 fractions were analyzed by SDS-PAGE and the Strep tag present on gB was detected by WB
1039 using Streptactin-HRP conjugate. The WT protein is found in the top fraction only in the
1040 presence of liposomes with 60% DOPC and 40% CH. **B) Co-floatation of WT gB and DOPC**
1041 **liposomes with increasing amount of cholesterol.** Liposome composition is indicated on the
1042 top. gB is detected in the top fraction only when 40% CH is present. **C) Co-floatation of WT gB**
1043 **and liposomes made of combinations of lipids found in plasma membrane.** The CH
1044 concentration was fixed to 40% or 0% (upper and lower panels, respectively), and one or two
1045 more lipids were added, resulting in total of 5 lipid compositions. The protein was detected
1046 bound to all of the CH-containing liposomes, while it was found in the unbound fraction in the
1047 absence of CH.
1048
1049 **Figure 4. A) Negative stain EM image of liposomes incubated with PrV gB ectodomains.**
1050 Characteristic hexagonal structures made of gB covering the liposomes (60% DOPC, 40% CH)
1051 are observed, representing the top view on the gB spikes. Individual trimers are establishing an
1052 extensive network of lateral interactions giving rise to the array appearance of the protein coat.
1053 Liposomes showing side views of the gB trimers projecting away from the liposome surface are
1054 marked with arrows. A blow-up of the area within the black rectangle is shown in the upper
1055 right corner. **B) Cryo-EM of PrV gB ectodomains bound to liposomes.** Arrows indicate
1056 individual gB trimers in which the 'top' end of the spike is better resolved, indicating that the

molecule binds to the liposomes via the other end i.e. the one carrying the FLs. Insert in the upper right corner depicts the shape of a gB trimer with the 'top' representing domain IV end of the spike, and 'FL' marking the base of domain I and location of FLs.

Figure 5. A) Sequence alignment of PrV and HSV-1 gB fusion loops regions. Identical residues are shown as white letters on red background, and residues with similar physico-chemical properties are colored in red on white background. Residues mutated in this study (*Trp187, Tyr192, Tyr267, Ile270, Phe275, Tyr276 and His277*) are boxed in green. Numbers 1-14 above the alignment designate the position of each residue in FL1 or FL2. The residues found to be important for binding to liposomes are indicated with vertical arrows and their corresponding numbers (3, 8 in FL1 and 9, 10 in FL2) are colored according to the scheme used in panel B. **B) Structural representation of the mutated PrV gB FL residues.** The aromatic residues in FL1 and FL2 are indicated with their side chains in stick representation. These residues were individually mutated as shown in Table 2. For clarity reasons the two views of the FLs are presented, and the remaining of the protein was omitted. The residues shown to be required for binding to liposomes are also indicated with their corresponding positions within FL1 and FL2.

Figure 6. SDS-PAGE analysis of purified PrV gB ectodomain variants. SDS-PAGE analysis of the PrV gB recombinant ectodomains under non-reducing (upper panel) and reducing (lower panel) conditions. 2μg of each purified protein were loaded on a 4-20% gradient gel. Proteins were stained with Coomassie blue stain. The three bands resolved under reducing conditions correspond to the uncleaved protein, the N-terminal and C-terminal fragments produced by

furin cleavage. There are no observable differences in purity and cleavage pattern between the FL variants and the WT PrV gB.

Figure 7. A) Liposome binding of PrV gB FL variants. WB analysis of gradient fractions, 't' - top fraction (liposomes and bound gB) and 'b'-bottom fraction (unbound protein). Liposomes were made of 60% DOPC and 40% CH. Arrows indicate presence of very weak signals in the top fractions observed for Y192F, Y267A and Y276F. Streptactin-HRP conjugate was used for gB detection. **B) Solvent-accessible surface representation of the bottom tip of the PrV gB spike carrying fusion loops.** ***Left panel:*** The FL residues mutated here are shown in the same colors as in Figure 4B. Star signs (*) indicate position of the conserved *Gly274*. The black contour designates the edges of the continuous, hydrophobic surface formed by the side chains of *Trp187, Tyr192, Gly274, Phe275,* and *Tyr276*. ***Middle panel:*** **Solvent-accessible surface colored according to hydrophobicity.** The same PrV gB surface as in the left panel is shown, with the colors corresponding to the hydrophobicity of the individual side chains and calculated using Eisenberg hydrophobicity scale (105), with white corresponding to the most hydrophobic, and dark yellow to the most hydrophilic/charged side chains. ***Right panel:*** **Electrostatic solvent-accessible surface.** The same surface as in the left panel is colored according to the electrostatic potential calculated by ABPS tool (106), with the blue and red corresponding to negative and positive potentials, respectively. All the images were generated in PyMol (104).

Figure 8. Expression of full-length PrV gB variants in RK13 cells (A) Subcellular localization. RK13 cells were transfected with expression plasmids for wild type gB (gB Ka) or the PrV gB FL

1101 mutants and analyzed by indirect immunofluorescence. One day after transfection, cells were
1102 fixed with 3% paraformaldehyde and permeabilized with 0.1 % Triton X-100. gB was detected
1103 using a gB specific rabbit antiserum and Alexa Fluor 488-conjugated secondary antibodies.
1104 Green fluorescence was excited at 488 nm, and recorded with a laser scanning confocal
1105 microscope (SP5; Leica, Mannheim, Germany). **(B) Western blot analyses.** Lysates of RK13 cells
1106 transfected with expression plasmids for wild type gB (gB Ka) or gB variants containing FL single
1107 point mutations were separated by SDS-PAGE under reducing conditions. Cells transfected with
1108 the empty vector pcDNA3 served as negative control (mock). The blots were incubated with the
1109 gB specific monoclonal antibody C15-b1. Signals of uncleaved gB (gB^a) or furin-cleaved gB
1110 subunit (gB^b) are labeled by arrows, and molecular masses of marker proteins are indicated. As
1111 loading control, the blot was incubated with an anti-alpha-tubulin monoclonal antibody.
1112
1113 **Figure 9. A) Functional data obtained for the PrV gB FL variants.** The results of the cell-cell
1114 fusion assay are plotted as black bars, and expressed as percent of the activity of the WT gB in
1115 combination with gH/gL which was set to 100% (left y-axis). Viral titers obtained in the trans-
1116 complementation assay are shown as grey bars, and correspond to the number of plaque-
1117 forming units (PFU) per ml (right y-axis). 'Ka' stands for PrV strain Kaplan and designates the WT
1118 protein, used as a positive control. The inverted triangles (▼) mark the three variants that
1119 showed poor binding to liposomes, while being functional in fusion and complementation
1120 assay. The ▲ triangle labels Y276A that had fusion-null phenotype in cell-cell assay, but was
1121 partially functional in the virus complementation assay. **B) Effect of liposome composition on**
1122 **binding of WT, Y192F, Y267A and Y276F PrV gB variants.** Two types of liposomes were used:

1123 '2L': 60% DOPC, 40% CH (left), and '4L': 20% DOPC, 20% DOPE, 20% SM and 40% CH (right), and
1124 the top ('t') and bottom ('b') fractions were analyzed by WB, showing higher amount of all the
1125 variants bound to the more complex '4L' liposomes. C) Floatation of PrV gB variants whose
1126 binding to liposomes is not affected by lipid composition. These variants showed the same
1127 binding pattern to '4L' liposomes, as for '2L' liposomes (Fig. 7A). Aliquots from the 'top' (t) and
1128 'bottom' fractions were analyzed by WB.
1129
1130 **Figure 10. Functional characterization of gB Δfurin. A) Western blot analysis**. Lysates of RK13
1131 cells transfected with expression plasmids for wild type gB (gB Ka) or the gB furin deletion
1132 mutant (gB-Δfurin) were separated by SDS-PAGE under reducing conditions. Cells transfected
1133 with the empty vector pcDNA3 served as negative control (mock). Blots were incubated with gB
1134 specific monoclonal antibody C15-b1. Signals of uncleaved gB (gB^a) or furin-cleaved gB subunit
1135 (gB^b) are labeled by arrows, and molecular masses of marker proteins are indicated. Signals of
1136 α-tubulin served as loading control. **B) Subcellular localization**. RK13 cells were transfected
1137 with expression plasmids for wild type gB (gB Ka) or gB Δfurin mutants and analyzed by indirect
1138 immunofluorescence. gB was detected using a gB specific rabbit antiserum and Alexa Fluor 488-
1139 conjugated secondary antibodies. Green fluorescence was excited at 488 nm, and recorded
1140 with a laser scanning confocal microscope (SP5; Leica, Mannheim, Germany). **C) Functional**
1141 **data**. Results from cell-cell fusion assay are plotted as black bars, and expressed as the percent
1142 of the signal measured for the WT protein set to 100% (left y-axis). The viral titers obtained in
1143 the trans-complementation assay are shown as grey bars, and correspond to the number of
1144 plaque-forming units (PFU) per ml (right y-axis). 'Ka' stands for PrV strain Kaplan and designates

1145 the WT protein, used as a control. pcDNA-3 transfected cells were used as negative control
1146 (mock).
1147
1148 **Figure 11. A) Hypothetical model of PrV gB ectodomain interactions with membranes.** The
1149 model displays the base of the PrV gB trimer, illustrating putative location of the FL residues
1150 investigated in this study, shown with their side chains as sticks, and colored as in Fig. 5B. The
1151 arrows and numbers are used to indicate the deeper insertion of *Phe275* (FL2-9) into the apolar
1152 region containing the lipid tails ('1'), and the 'interfacial rim' made of *Tyr192, Trp187, Tyr276*
1153 ('2') (FL1-8, FL1-3, FL2-10) that would be located within the more polar part of the membrane.
1154 A single molecule of DOPC and its putative localization in the membrane is shown in stick
1155 representation on the right. Carbon, oxygen, phosphorous and nitrogen atoms are colored as
1156 white, red, orange and blue. **B) Hypothetical model of HCMV and EBV gB interactions with**
1157 **membranes.** HSV-1 (PDB 2GUM), HCMV (PDB 5CXF) and EBV gB (PDB 3FVC) structures were
1158 superposed onto the PrV structure using Dali pairwise alignment algorithm (107). The latter two
1159 structures contain WT resides (YIY$^{155\text{-}157}$ and WLY$^{240\text{-}242}$ in HCMV, WY$^{112\text{-}113}$ and WLIW$^{193\text{-}196}$ in
1160 EBV gB) that were modeled back onto the FL residues that had been mutated in the crystallized
1161 constructs (GHR$^{155\text{-}157}$ and ATH$^{240\text{-}242}$ in HCMV, and HR$^{112\text{-}113}$ and RVEA$^{193\text{-}196}$ in EBV). The
1162 residues at positions FL1-8, FL1-3, FL2-10 and FL2-9 are indicated and colored as in Fig. 5B, with
1163 their side chains shown as sticks. *Trp* found at FL2-8 in HCMV and EBV gB are colored in salmon,
1164 and *Tyr* side chains at FL1-10 and FL1-7 positions in HCMV and EBV gB are colored in light blue.
1165 Grey transparent boxes are highlighting the putative interfacial rim in each structure. The side
1166 chain of *Trp*^{193} inserted between FL2-5 and FL2-6 residues in EBV gB is labeled as 'FL2-5*6' and

colored in magenta. Other hydrophobic residues are not shown as sticks for clarity reasons. **C) Sequence alignment of the FL regions.** Residues with similar physico-chemical properties that are 75% or more conserved are colored in red. Secondary structure elements corresponding to the PrV gB ectodomain structure are displayed on the top, and resides identified as membrane contact sites in PrV gB (FL1-3, FL1-8, FL2-9 and FL2-10) are indicated with black arrows. The numbering on the top corresponds to that of the PrV gB protein. The alignment was generated in Clustal Omega (108) and displayed using ESPript (109).

Figure 12. Conservation of gB in alphaherpesviruses plotted on the PrV gB ectodomain structure. A) Solvent-accessible surface of PrV gB in multiple orientations is shown. Residues showing identity lower than 75% are colored in white, while the residues that are strictly conserved in more than 75% of the analyzed sequences are colored in increasing purple gradient. The alignment shown in supplemental material Fig. S1 was used. **B) PrV gB FLs.** Fusion loop residues investigated in this study are shown with the side chains in stick representation. Two orientations are presented for clarity reasons.

Table 1. X-ray diffraction data collection and refinement for PrV gB

X-ray data processing			
Beamline	ESRF ID23		
Space group	H3		
Cell constants a, b, c, α, β, γ	99.89 Å 90.00°	99.89 Å 90.00°	272.89 Å 120.00°
Resolution (Å)	46.15-2.69 (2.85-2.69)[a]		
No. of reflections	147396 (23196)		
Multiplicity	5.3		
<I/σ(I)>	14.99 (2.33)		
Completeness (%)	99.6% (98.3%)		
R_{merge}	7.4% (52.3%)		
R_{pim}	5.5% (38.6%)		
$CC_{1/2}$	0.98 (0.82)		
Wilson B factor (Å^2)	55.7		
Refinement			
Program	BUSTER 2.10.2		
Resolution (Å)	46.15-2.70 (2.80-2.70)		
No. of reflections	27695 (2738)		
R_{work}/R_{free}[b]	0.193 / 0.236		
No. of atoms[c]	4759 / 92		
B-atomic factors (Å^2)[d]	73 / 73.8 / 59.6		
Geometry			
rmsd bond lengths (Å)	0.010		
rmsd bond angles (°)	1.16		

Ramachandran plot[e] (%)	95.25 / 4.24 / 0.51

[a] – Outer-shell values are given in parentheses

[b] – R_{free} test set was composed of 5% randomly chosen reflections

[c] – Refers to number of protein / water atoms

[d] – Refers to overall / protein / water B-factors

[e] – Preferred / allowed / outliers as calculated by Coot

1193 **Table 2. PrV gB mutants with single point mutations in fusion loops in liposome binding and**

1194 **functional assays.**

	PrV gB variant	Binding to 2L[a] liposomes	Cell-cell fusion	Trans-complement.	Binding to 4L[b] liposomes	Ectodomain yield /protein purity[c]
FL1	W187A	-	-	-	-	n.c.
	W187H	-	n.t.	n.t.	-	n.c.
	W187F	-	n.t.	n.t.	-	n.c.
	Y192A	-	-	-/+	-	n.c.
	Y192F	-/+	+	+	+	n.c.
FL2	Y267A	-/+	+	+	+	n.c.
	Y267F	+	n.t.	n.t.	+	n.c.
	I270A	+	+	+	+	n.c.
	F275A	-	-	-/+	-	n.c.
	F275W	+	+	+	+	n.c.
	F275Y	-	-	-/+	-	n.c.
	Y276A	-	-	-/+	-	n.c.
	Y276F	-/+	+	+	+	n.c.
	H277A	+	+	+	+	n.c.
	H277W	+	n.t.	n.t.	+	n.c.

1195

1196 Single point mutations introduced in the FL1 and FL2 of PrV gB are indicated. Sign '-/+' in the

1197 second column designates presence of a faint band in the liposome fraction (Fig. 7A), indicating

1198 weak binding of the protein to liposomes, or in the fourth column, marginal complementation

1199 of PrV-ΔgB virus (Fig. 8A). Highlighted in grey are the variants containing mutations to alanine.

1200 'n.t.' stands for not tested.

1201 [a] – 2L indicates that liposomes were made of 2 lipids: 60% DOPC, 40% CH

1202 [b] - 4L indicates that liposomes were made of 4 lipids: 20% DOPC, 20% DOPE, 20% SM, 40% CH

1203 [c] – expression yield and purity of the recombinant ectodomains is indicated relative to the WT

1204 protein; 'n.c.' stands for 'no change'.

Table 3. Sequence and structural comparison of PrV gB and HSV-1 / CMV / EBV ectodomains

	Sequence identity (%)[a]	n_A/n_T[b]	rmsd (Å)[c]
PrV vs HSV-1	50.1	524/568	1.04
PrV vs CMV	25.6	508/535	3.39
PrV vs EBV	25.3	496/530	3.72

[a] – percent identity has been calculated using the shorter sequence as denominator

[b] – n_A and n_T indicate, respectively, the number of aligned and total atoms

[c] – the root-mean-square deviations (rmsd) were calculated for Cα atoms in PyMOL (104)

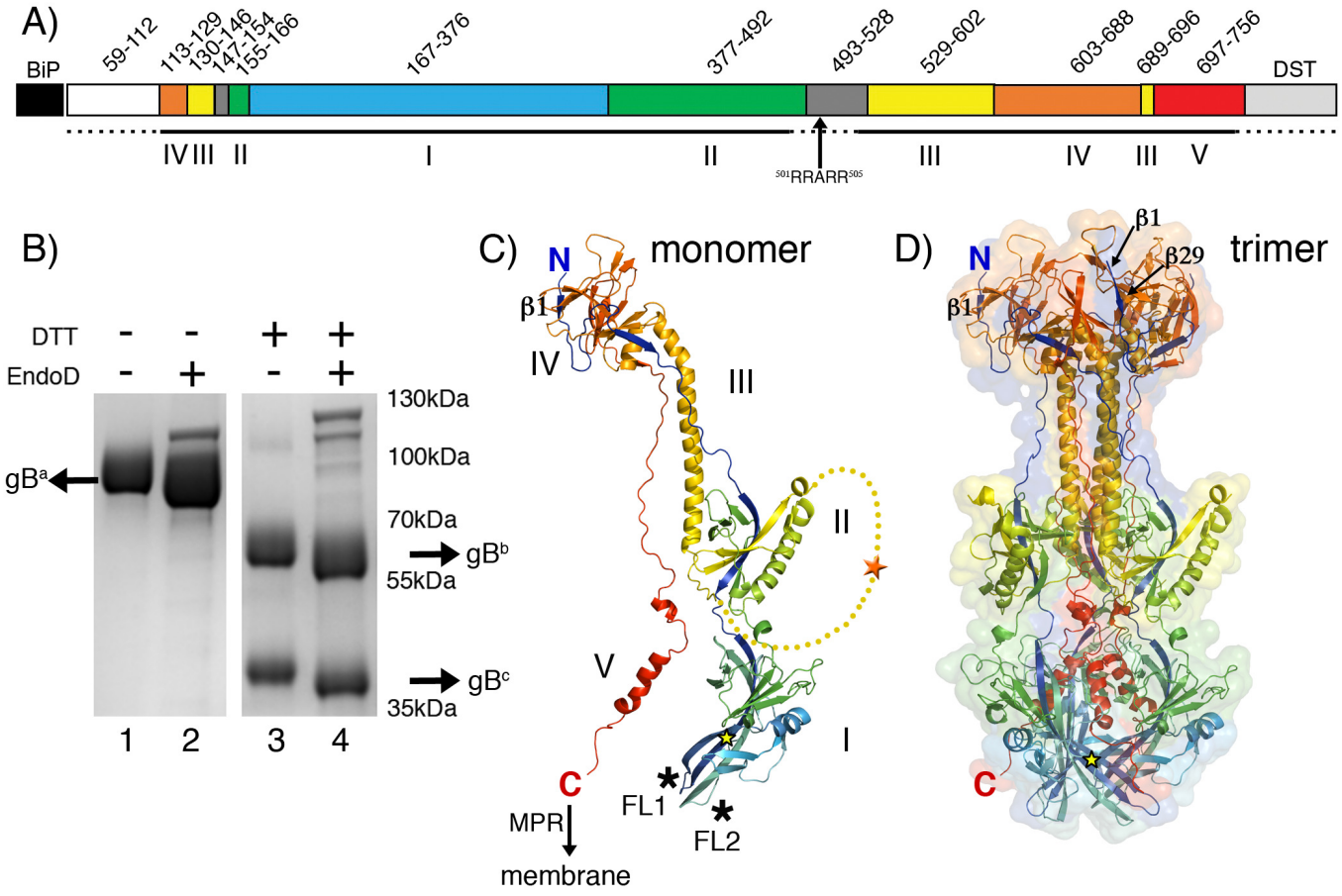

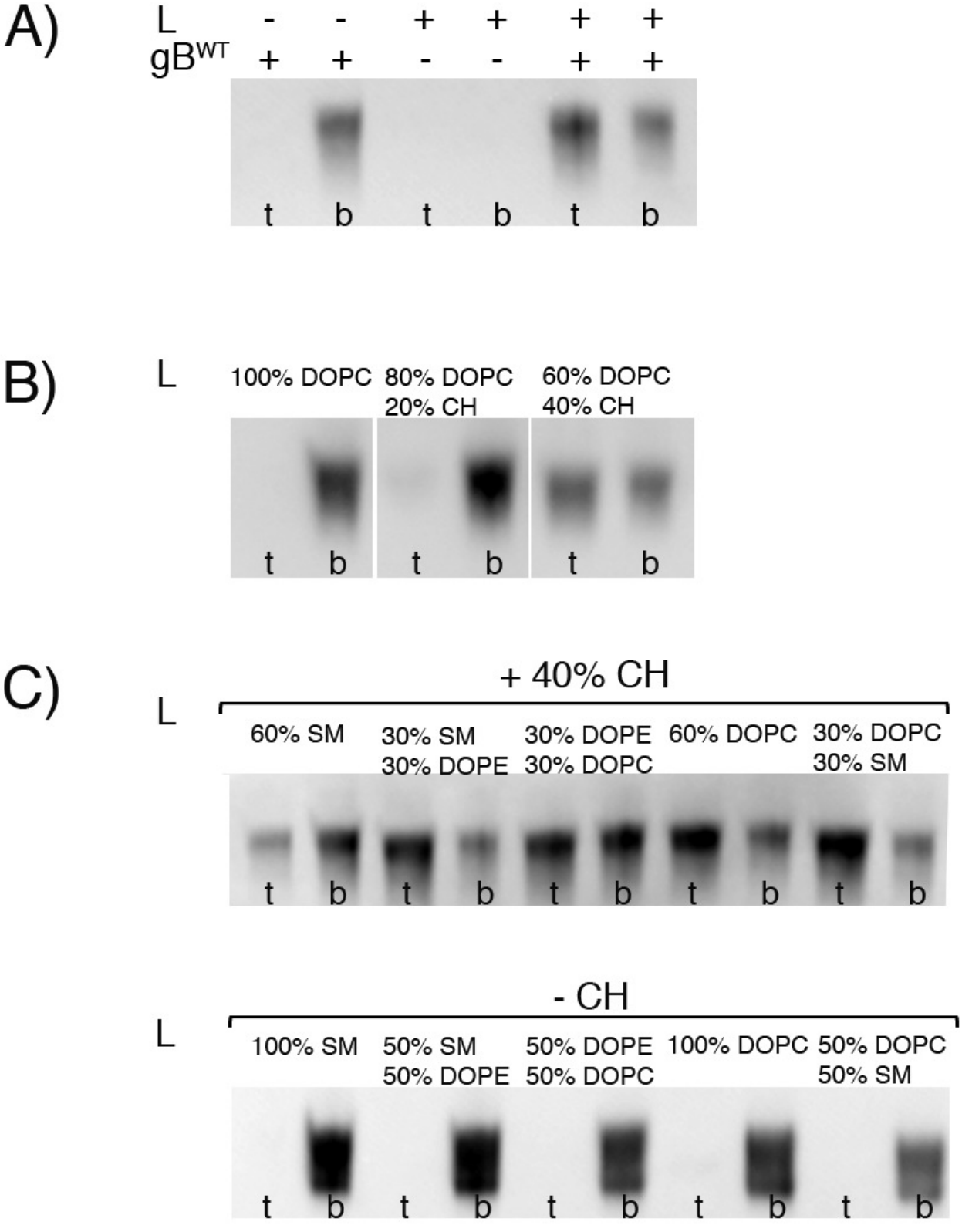

Journal of Virology

JVI

Journal of Virology

A) Negative stain

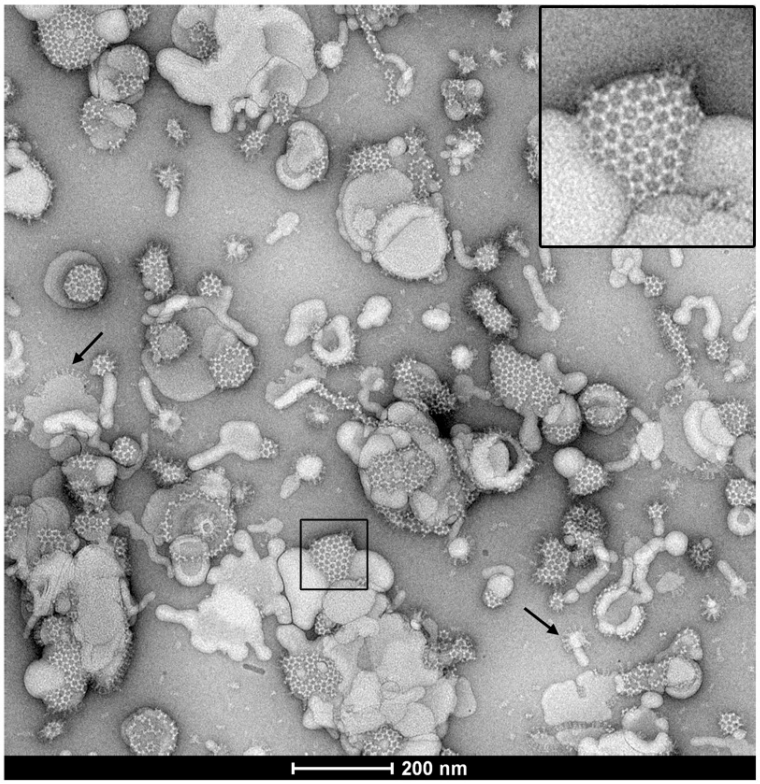

B) Cryo-EM

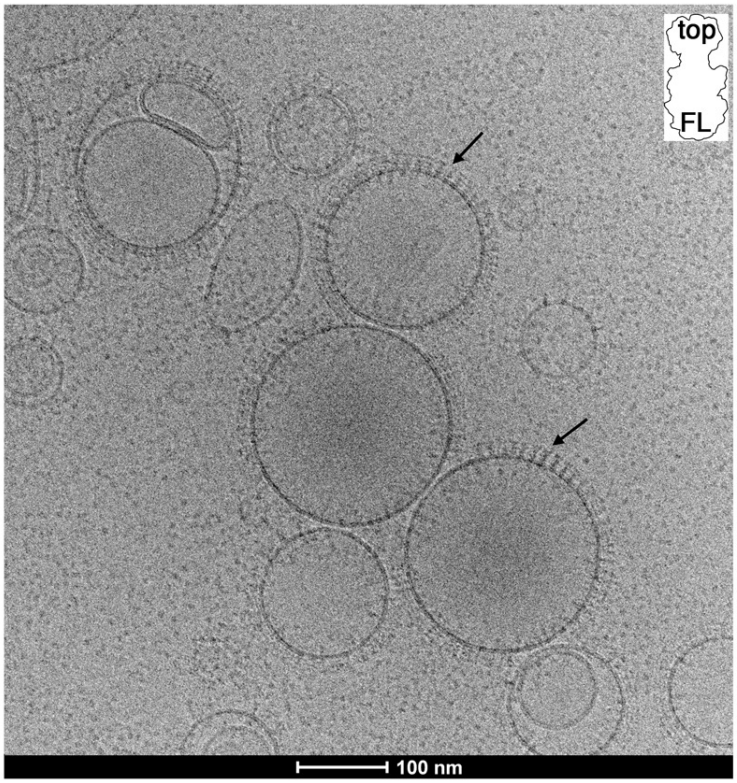

A)

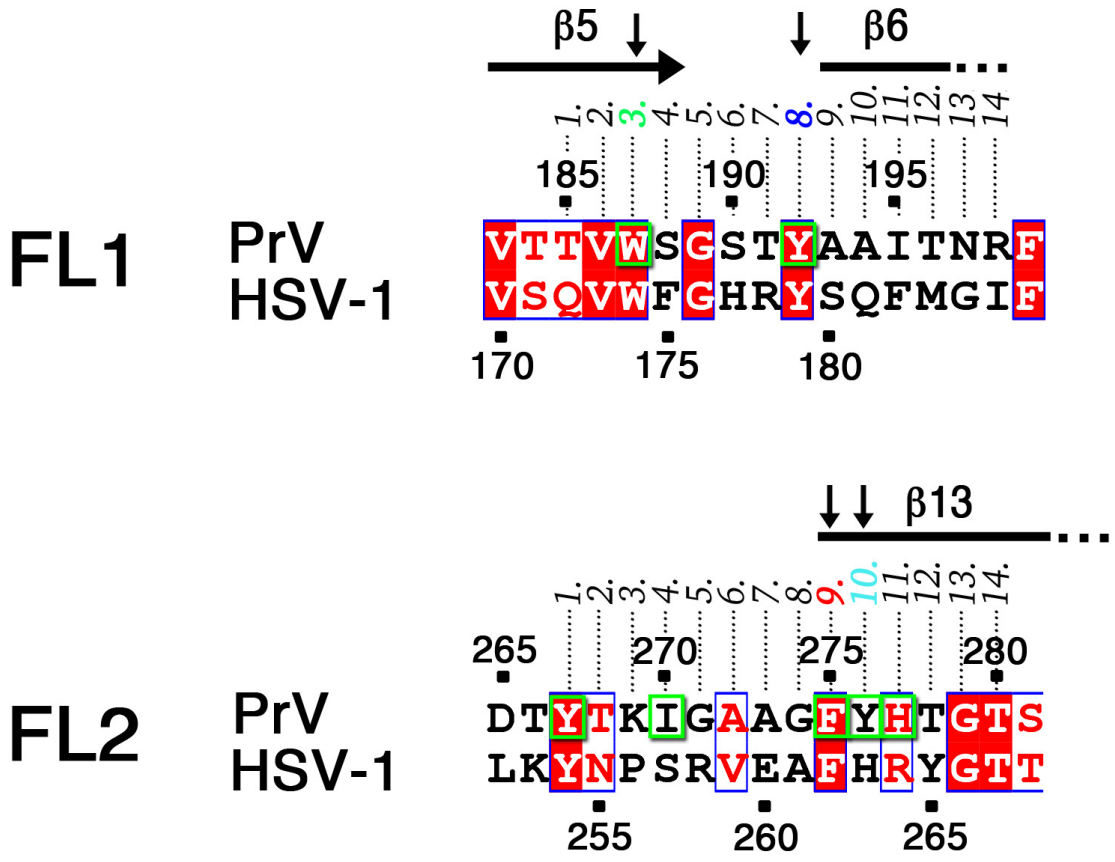

B)

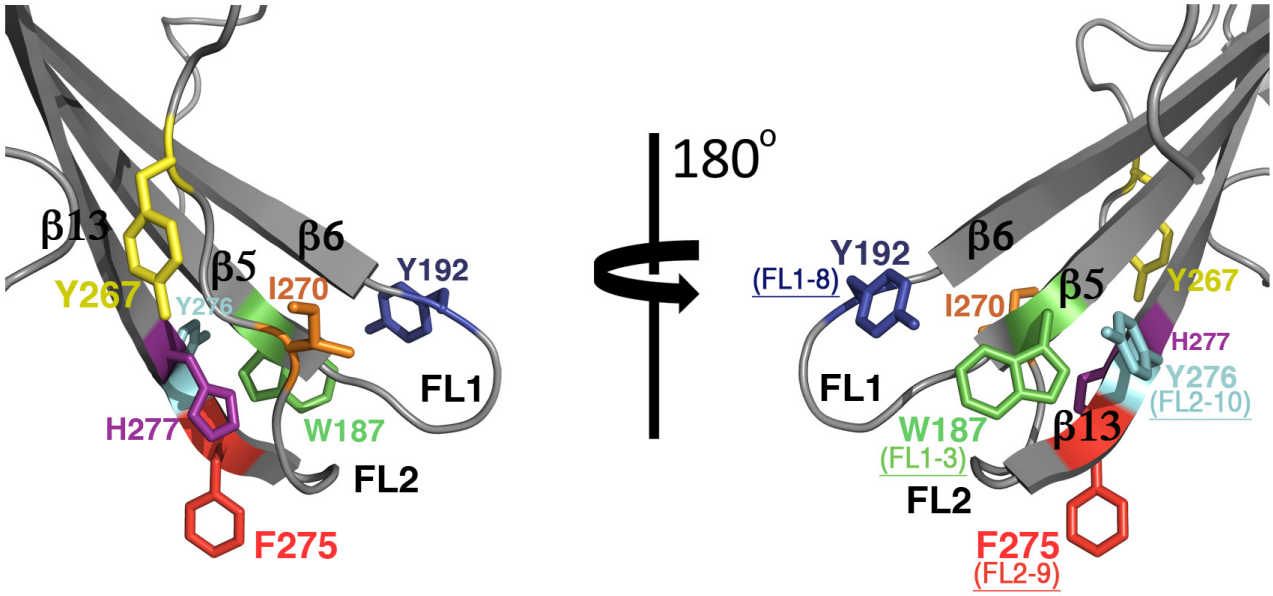

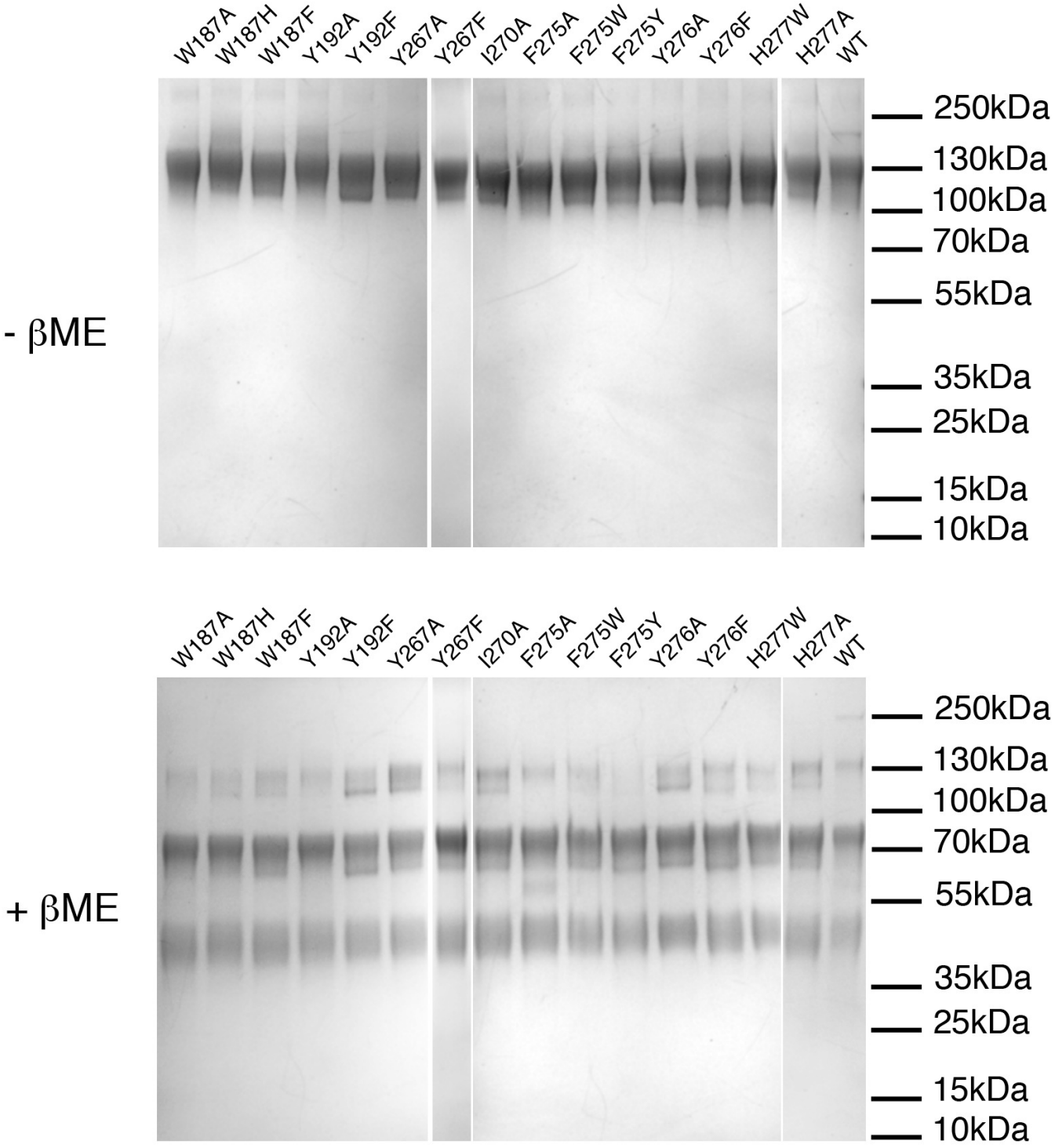

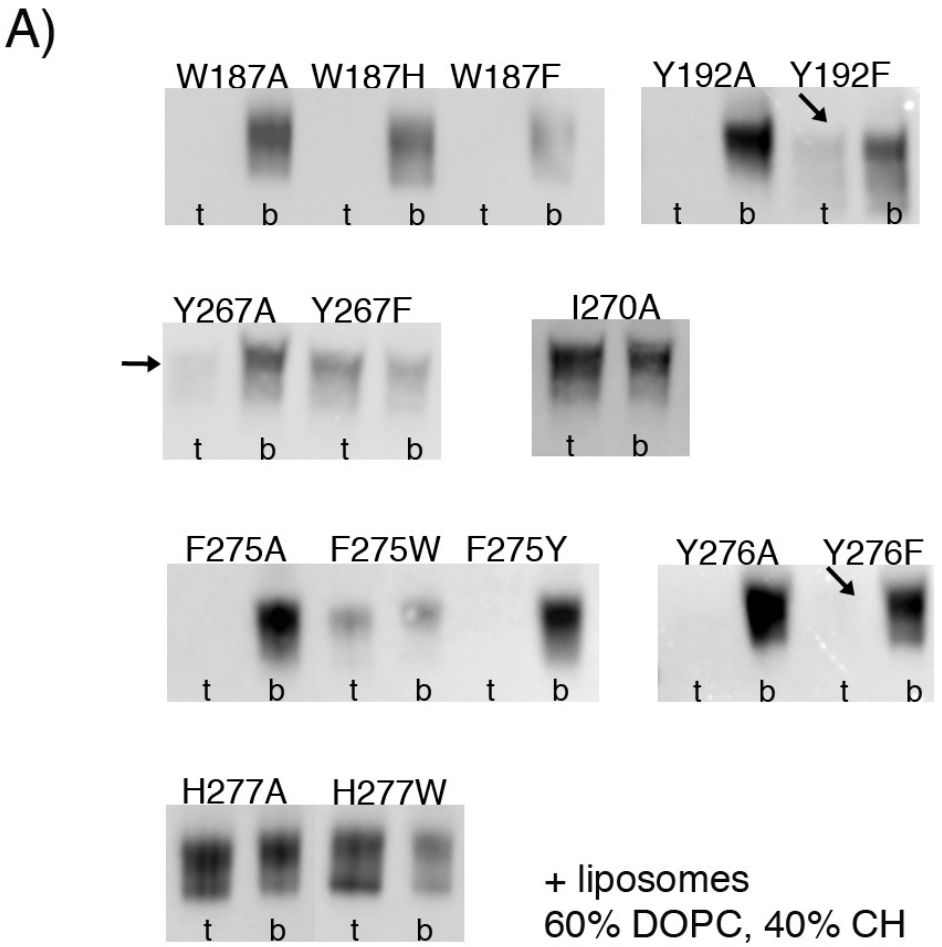

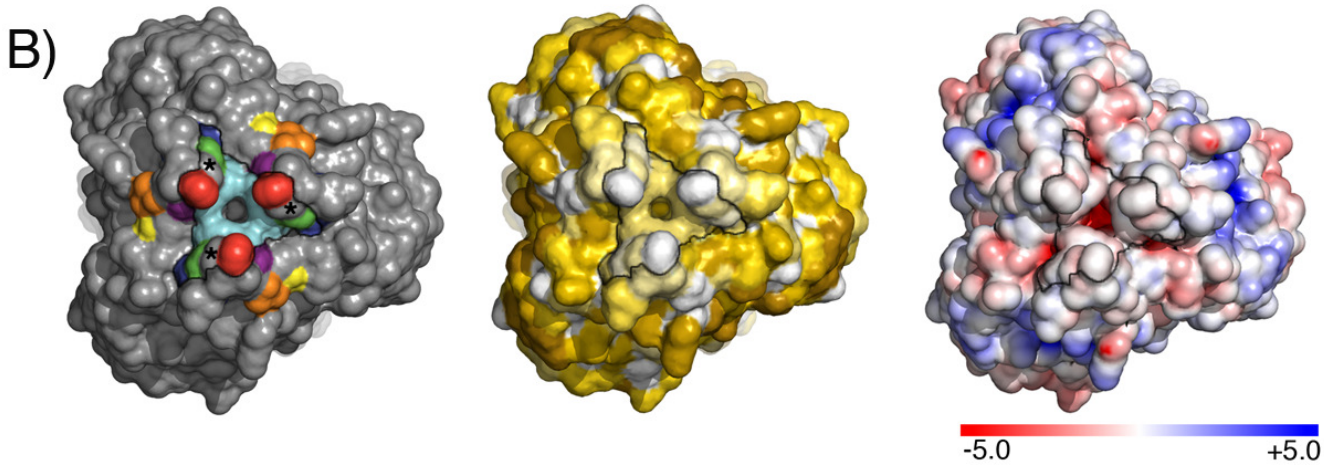

A)

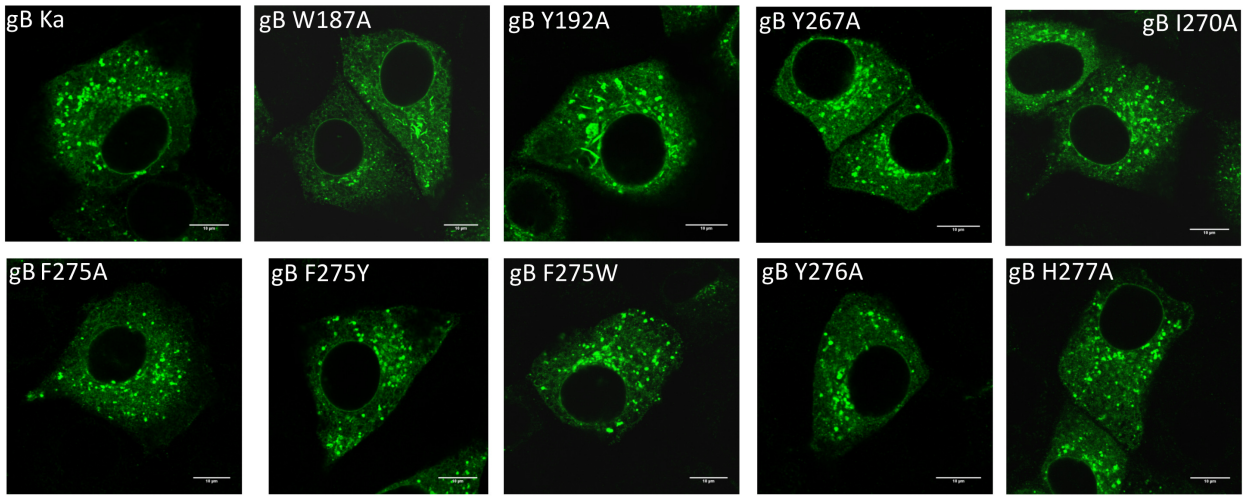

B)